

Thermal imaging as a method to study the effect of induced ischemia on vasomotion

ANNABEL BANTLE, CHRISTIAN KORFITZ MORTENSEN, TOBY STEVEN WATERSTONE

December 20, 2017

Abstract

Vasomotion is an autoregulatory mechanism that optimizes blood distribution within the microcirculatory system. Thermal imaging is a promising approach to measure this phenomena. Previous studies have found that vasomotion is quantifiable as temperature micro oscillations in the endothelial (0.005 - 0.02 Hz), neurogenic (0.02 - 0.05 Hz) and myogenic (0.05 - 0.15 Hz) frequency band. Four healthy subjects were recruited to investigate the possibilities of measuring changes in vasomotoric activity caused by partial brachial occlusion of blood supply by using thermal imaging. Measurements were done as a baseline and with 50% restriction of the hand's blood supply by a brachial cuff. Data processing involved correction of artifacts seen in the temperature recordings. Morlet continuous wavelet transform was used on the corrected temperature recording to find the frequency content in the micro temperature oscillations. A paired t-test within the frequency bands showed no significant difference between the mean magnitude values of baseline (endothelial 6.71 ± 1.90 , neurogenic 5.05 ± 0.65 , myogenic 4.66 ± 0.77) and restriction (endothelial 5.95 ± 0.75 , neurogenic 4.82 ± 0.95 , myogenic 4.70 ± 0.72). Results show thermal imaging might not be sensitive enough to detect changes in vasomotion during a 50% restriction of blood supply, and limitations in the experimental setup.

I. INTRODUCTION

The use of thermal imaging to study the phenomena of vasomotion might present a new biomarker for the treatment of patients going into shock.[1,2] Vasomotion is the phenomena of oscillating changes in the capillary vessel diameter enforced by smooth muscle cells. This phenomena occurs in the microcirculatory system as an autoregulatory mechanism that optimizes blood distribution within the microcirculatory system.[3-6] Changes in micro temperature oscillations are the source of thermal waves, from the blood flow, propagating from microvessels toward the skin surface.[7] Although several studies have investigated the occurrences of vasomotion within the capillary network, only few have used thermal imaging as detection method.[8-10] With a better knowledge of vasomotion it might

possible to give an earlier prediction, if patients are developing shock. Particularly patients who are in danger of developing hypoxia due to shock, as this affects alterations in the microcirculatory system and interfere with the perfusion.[1,2] New methods for studying vasomotoric activity arise and thermal imaging presents advantages in larger sample area and by being non-invasive. Previous studies detected that the vasomotoric blood flow is quantifiable as micro temperature oscillations within three frequency bands of endothelial (0.005 – 0.02 Hz), neurogenic (0.02 – 0.05 Hz) and myogenic (0.05 – 0.15 Hz) origin.[3,7-9] The significance of these frequency band during disease are for instance shown in a decrease in amplitude of endothelial blood flow oscillations which assumed to be a biomarker for endothelial dysfunction, which indicate cardiovascular disorders such as arterial hyper-

tension and cardiac ischemia.[7] Therefore the interest of this study was to investigate thermal imaging's ability to detect, if there are changes in the micro temperature oscillations depending on hypoxia in the microcirculatory system.

II. METHODOLOGY

i. Subjects

Four healthy subjects, 3 males and 1 female, average age 30.5 ± 12.5 years were recruited. Two subject were right handed and two left handed. No subjects consumed caffeine, alcoholic beverages, or medicine before the experiment. All subjects were aware of the experimental procedure and were willing to participate. Subjects showed no signs of cardiac disease or tremors.

ii. Test setting

Subjects were placed in an upholstered adjustable chair for a comfortable sitting position. The hand was stabilized by a vacuum pillow covered with micro fiber tissue, which was attached on the armrest. Xenics Gobi 640 $17\mu m$ GigE infrared camera (Xenics NV, Belgium), sensitivity $0.05^\circ C$, resolution 480×640 , was positioned with a tripod 37.5 ± 1.0 cm over the subject's dominant hand and connected via Ethernet cable with a computer (figure 1).



Figure 1: The experimental setup at Region Hospital Nordjylland.

iii. Software setting

Xeneth 2.6 software (Xenics NV, Belgium), installed on a computer, was used for data acquisition. The sampling rate was set to 6.25 Hz, the file format to a raw data xvi-file and both, room and ambient temperature, to $25^\circ C$ and emissivity of observed object to 1.

iv. Experimental procedure

2×20 min data acquisition periods were planned. One as a baseline, and another where blood flow restriction enforces hypoxia[4]. The camera was set to warm up for at least 15 min. Meanwhile systolic blood pressure was measured to determine total occlusion pressure (TOP) of the subject's dominant arm. Needed brachial cuff pressure (p_{cuff}) for restricting 50% blood flow is 30% of the TOP. TOP was calculated with $p_{cuff} = TOP \times 0.3$.[11] The subjects had at least 30 min to adjust to the room temperature.

The brachial cuff for enforcing blood flow restriction in the second acquisition period was affixed on the subject's dominant arm without tightening it before both measurements. The subject was placed in the chair and the dominant hand was stabilized with the vacuum pillow. The lens was adjusted, so the hand was in focus.

To minimize any possible movement bias the subject was not allowed to move or speak during the whole procedure.

v. Data processing

v.1 Preparation of data

The acquired xvi-files were read and processed in MATLAB R2017b. The header in the beginning of each file and frame was removed. Afterwards the raw uint 16 pixel intensities were divided into frames.

v.2 Regions of interest

28 regions of interest (ROIs) were selected on behalf of getting full representation of the hand

(figure 2). Each region represented one pixel intensity in the 640×480 image matrix.

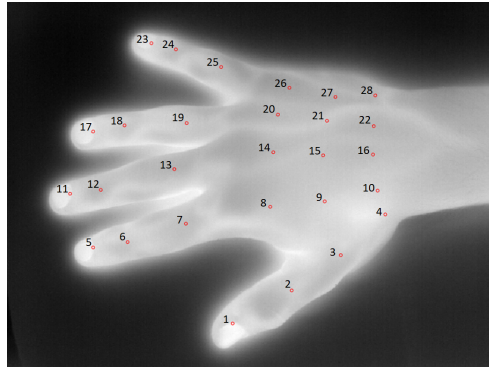


Figure 2: Frame from thermal image of subject 1. Red dots are indicating the 28 ROIs, with respective numbering.

This pixel represented an area of the hand with a width of approximately $417\mu\text{m}$.

v.3 Artifacts

Under visual inspection of the temperature trace over time, some unexplainable discontinuities were present. These discontinuities were characterized as artifacts made by the camera[12,13]. From the raw data of all regions, three types of artifacts were characterized. A white noise component is observed during the whole recording, intervals between two discontinuities containing a drift component and adjustments by the shutter from non-uniformity correction due to the drift component. All artifacts are shown in figure 3, which is representing one temperature trace from a region. The artifacts are assumed to occur because each microbolometer in the focal plane array has a different response to the same infrared excitation. This caused the camera to perform non-uniformity corrections, where all microbolometers are re-calibrated, resulting in an offset.[12,13]

v.4 Correction method

The shutter adjustments and the drift between these adjustments, seen in figure 3, corrupted

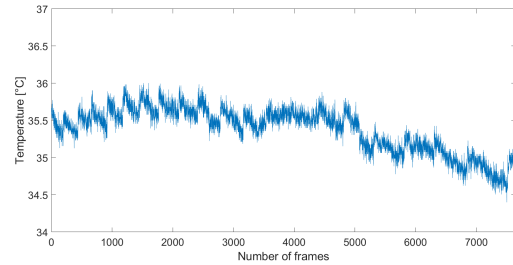


Figure 3: Raw temperature trace in relation to frame number of region 15 in baseline recording of subject 1, showing outline of the artifacts as discontinuities.

the raw temperature trace the most. Therefore a correction method based on linear regression was implemented. The linear regression was made on each drift between shutter adjustments. The regression lines were put together at the middle point of an adjustment forming a new temperature recording base. Figure 4 shows how the residuals are projected on to the newly corrected base forming a new temperature trace.

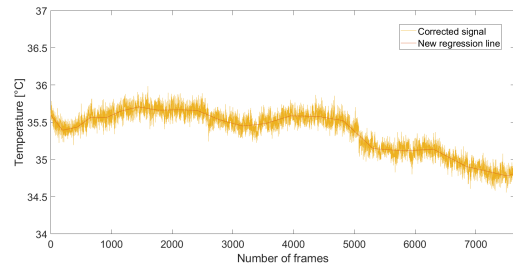


Figure 4: New oriented regression line based on temperature trace of baseline recording from subject 1 in ROI 15 plotted in red. Corrected temperature trace of the same baseline recording plotted in yellow.

v.5 Time-frequency analysis

Analysis of the corrected data was done in the time frequency domain by the use of Morlet continuous wavelet transform (CWT). The CWT present higher resolution of frequency content in low frequency signals, compared to the Fourier transformation.[7,8]

In the CWT, the signal is convoluted with the Morlet wavelet in equation 1:

$$W(\tau, s) = \int_{-\infty}^{\infty} x(t) \frac{1}{\sqrt{|s|}} \psi * \left(\frac{t - \tau}{s} \right) dt \quad (1)$$

Where $x(t)$ is the signal and ψ is the Morlet wavelet. W denotes the wavelet transformation magnitude in relation to the time τ and frequency s . A scalogram showing the time-frequency content of the uncorrected temperature trace given as output of the CWT can be seen in figure 5.

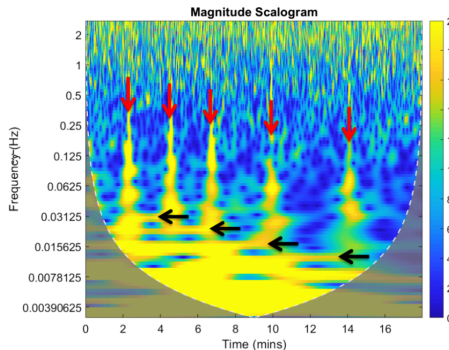


Figure 5: Scalogram from subject 3 in ROI 8, uncorrected baseline recording. Red arrows showing frequency content of discontinuities in the temperature trace and black arrows showing frequency content of drift artifacts.

The discontinuities within the temperature trace are clearly shown as high magnitude spikes in the scalogram. In figure 5 those spikes are marked with red arrows. The black arrows mark the drift that is contained in between each discontinuity, as seen the drift decrease in frequency.

After application of the correction method, each temperature trace and its corresponding scalogram were submitted a manual control. During this control it was noticed that some temperature traces still contained discontinuities which hampered correct data analysis for those temperature traces. Five ROIs have been chosen valid for further data analysis. The criterion for this selection was, that those ROIs showed good response to the correction method and no discontinuities visible in the

scalogram. The five selected ROIs were 10, 14, 20, 21 and 22, those can be seen in figure 2. The corrected temperature trace from figure 5 is shown in figure 6, which is also illustrating the frequency bands of interest.

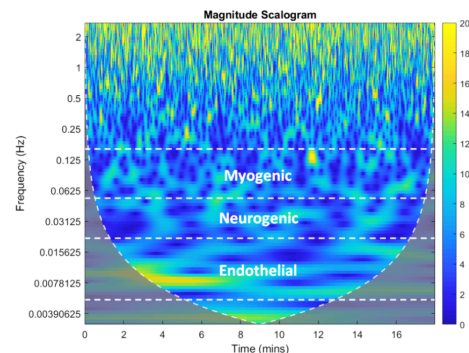


Figure 6: Scalogram from subject 3 in ROI 8, corrected baseline recording. Frequency bands of endothelial, neurogenic and myogenic are shown.

The combination of a valid corrected temperature trace across all subjects corresponding to the same ROI is needed for equally comparison between subjects, why only five regions could be used for further data analysis.

vi. Statistical approach

The magnitude within the scalograms of both conditions was compared for each subject. This comparison was conducted for the five ROI within the endothelial, neurogenic and myogenic frequency band. In every recording one mean magnitude value was calculated for each frequency band.[14] To test the statistical significance of the difference between the mean magnitudes a paired t-test has been applied.

III. RESULTS

The box plots shown in figure 7 (appendix) display the mean magnitude of each frequency band for each subject ordered by color in both conditions. The line connecting baseline and restriction condition indicates if the magnitude increased or decreased.

Throughout the combination of frequency band and regions, no clear pattern is visible for the four subjects. In each frequency band the mean magnitude both increase and decrease for each subject. Only subject 2 shows a clear pattern before and after the intervention, where mean magnitude seem to decrease in every frequency band and region.

Table 1 illustrates a mean magnitude value for endothelial, neurogenic and myogenic frequency band in the baseline and restricted measurement. The mean magnitude values are representing all subjects and ROIs.

Table 1: Table showing the mean magnitudes of each frequency band in both measured conditions.

	mean endo	mean neuro	mean myo
Baseline	6.71±1.90	5.05±0.65	4.66±0.77
Restriction	5.95±0.75	4.82±0.95	4.70±0.72

With the values visualized by the box plots in figure 7 a paired t-test provided the following p-values (table 2).

Table 2: Table showing the p-values corresponding to specific ROI in correlation with frequency band.

	p-endo	p-neuro	p-myo
ROI 10	0.71	0.93	0.84
ROI 14	0.62	0.69	0.92
ROI 20	0.41	0.80	0.84
ROI 21	0.40	0.84	0.95
ROI 22	0.38	0.15	0.93

IV. DISCUSSION

This study investigated the hypothesis, if thermal imaging is sensitive enough to measure the effects of vasomotion activity, and thereby investigate if changes in the microcirculatory system caused by a 50 % restriction of blood flow occur.

i. Results

The obvious assumption, based on the presented p-values, that there are no changes in the microcirculatory system or rather in vasomotion by 50% restriction of blood flow could

be due to incorrect brachial occlusion. Incorrect occlusion would yield insufficient restriction for affecting the microcirculatory system in a measurable way. The systolic blood pressure measurements, for determining the total occlusion pressure needed for brachial blood flow restriction of three subjects, showed high values around 140 mmHg and 150 mmHg outside the normal, which is around 120 mmHg for the systolic blood pressure[4]. Since those three subjects were in different age and shape, a suspicion for incorrect values arise. Even if the blood pressure monitor delivered incorrectly high values, the outcome of the restriction period would not have been influenced negatively. This would only lead to a calculated occlusion pressure higher than the one needed to reach the intended restriction, which would just lead to a larger difference between both conditions. It would be more problematic with an occlusion level too low. Furthermore all blood pressure measurements were conducted and verified by a professional anesthesiologist. The measured blood pressure values and occlusion pressure can be seen in table 3 in the appendix.

An interesting question to rise, is whether or not any vasomotion has been measured in the recordings. A prior study found mean magnitudes of 3.52 and 4.73 for endothelial, 3.73 for neurogenic and 2.96 myogenic frequency band[14]. Comparing these finding to this study's baseline means of 6.71, 5.05 and 4.55, it is seen that this study found a greater magnitude in every corresponding band. It is assumed that vasomotion contributes to the measured activity, and the higher magnitude in this study might be induced by remaining artifacts. The mean values that the paired t-test is based on, are extracted from the CWT data in the specific frequency bands. Though the cone of influence (COI), displayed in the scalograms as gray fading, has not been taken into consideration. The areas outside of the COI mark regions of the CWT containing areas of uncertainties, because of the bigger window size needed for the computation of the lower frequency content[14].

The use of the paired t-test was mainly due to the study design, where it is determined if there will be a significant difference in vasomotion, between the baseline and the restriction, within subjects. It was assumed that the data was normal distributed because of a natural variance within the population, why a parametric test was used. But with the small sample it was not possible to determine the actual distribution. In case of non-normally distribution a non-parametric test should be used. In this case a Wilcoxon signed rank test would be the approach for the statistical test. This test does not require a normal distribution in the population and is focusing on the population median value instead of the population mean like the paired t-test[15].

ii. Critique of study design

The small sample size of four subjects applied to the statistical methods are not sufficiently meaningful. With a larger amount of subjects this study would get a more representative result. Originally a larger amount of subjects was planned to be recruited for the experiment. However, the notice of artifacts in the temperature trace lead to the choice of not recruiting more subjects. Instead the focus was put on finding the origin of these artifacts and a way to bypass these. Instead of trying to bypass these artifacts in the data processing, other experiment testing camera operation in more controlled settings could have been carried out. Furthermore the statistics might not have led to any valid results with these artifacts in the temperature trace, even with a greater amount of subjects.

Stabilizing the subject's hand by a vacuum pillow was done with the assumption that the subjects were still, but this does not give sufficient support to inhibit every movements of the subject. A mechanism for better stabilization of the hand should be included. Else image alignment in the data processing to limit the drawbacks of possible movements in the recordings could have been included. Furthermore with the used setup exact same conditions for each

subject cannot be granted. For instance the ambient temperature might have had an effect on the recording. It is noticed that subject 1 had a skin temperature of around 38°C compared to the skin temperature of around 26°C of subjects 2 and 3. Both were having cold hands during the baseline recording. Looking at the ambient temperature in the recordings of areas outside of the hand stating a temperature of 25.83 ± 0.99 °C, being highest at subject's 1 recording. Other explanations than the room temperature, for the great difference in subject hand temperature should be considered, like mental state of the subjects and activity prior to the experiment. The software settings should be verified and if necessary changed beforehand of the experiment to fit the circumstances. An optimization of the test setting would require a more controlled setup of the experiment and a thermal camera of higher quality preferable of a cooled type.

iii. Limitations in using thermal camera

Due to the corrupted temperature reading the correction method was implemented, which clearly affects parts of the temperature trace in specific ROIs. The pixel drift increases with increasing distance to the center of the thermal image why pixel drift of ROIs located in the outer areas of the thermal image cannot be completely compensated with the implemented correction method[13]. The correction method shows another weak point in correcting the drift when the hand's overall temperature changed during a recording. The explanation for both is likely that the correction method was based on the assumption that the drift component in every interval is linear[13]. If the drift component is linear, the correction method works fine for linear temperature traces. Though this assumption borders the correction of non-linear temperature traces by enhancing discontinuities. The limitation of correcting temperature traces with an overall temperature change arise the suspicion that the correction method might rule out the mi-

cro oscillations in temperature. Besides, the assumption of a linear drift component might be wrong and a correction method that uses another regression method or combines different regression methods might adjust the artifacts in a better way. Another camera might also be preferable to reduce the risks of technical artifacts like these. It should be noticed that in the baseline recording of subject 2, no discontinuities occurred. This subject is the only in which there can be seen a pattern as a decrease in the mean magnitude of all the frequencies bands from the intervention, this is further illustrated on figure 7. If no discontinuities had been present, the general tendency of the mean magnitudes from the data might have looked different, assumable with a decrease in mean magnitude like in subject 2's case.

Furthermore the closer the thermal camera to the observed area, the smaller the area represented by one pixel. Within this study one pixel represents an area with a diameter around $417\mu\text{m}$. Capillaries have an average diameter of $8\mu\text{m}$ [14]. As the interest lies in observing several capillaries within a capillary bed, a ROI should be larger than the diameter of one capillary. But with the use of a too large ROI, it might be that the amount of inverse dilating capillaries is equal and thereby canceling each other out. Due to inverse dilating capillaries there might be no changes over time measurable because the frequency contents are occurring alternating in the different capillaries. In addition, the artifact content in the temperature trace was significantly higher than in the temperature traces detected in previous studies. Comparing the temperature traces, the question arises, if the artifacts overlap or suppress the frequency content of vasomotoric activity. Even though temperature changes over time in the skin were detected, it is uncertain, if this temperature traces just represents the general skin temperature or also vasomotoric activity.

V. CONCLUSION

The results of this study indicate that thermal imaging is not sensitive enough for detecting

changes in vasomotion during a 50% restriction of blood supply. No statistical significant difference between the two conditions was found, indicated by the p-values in table 2. Despite no findings, this study provides information about key points that should be considered when studying vasomotion with thermal imaging. For instance that the regions of most interest should be placed in the center of the thermal image to reduce drift as much as possible, and the importance of thermal camera specification. Further investigation in this field is needed, to investigate if thermal imaging is a promising technique for detecting changes in vasomotion.

VI. ACKNOWLEDGMENT

The authors would like to thank Lasse Riis Østergaard, Carsten Dahl Mørch and Andrei Ciubotariu for the cooperation and great advice during this study. Furthermore we are Region Hospital Nordjylland thankful for the use of their facilities during the experiment.

REFERENCES

- [1] Ronald V. Maier. Approach to the Patient with Shock. In: Harrison's Principles of medicine 18 (2012). url: <http://accessmedicine.mhmedical.com/content.aspx?bookid=331%7B%5C%7Dsectionid=40727056>.
- [2] Can Ince. The microcirculation is the motor of sepsis. In: Critical care (London, England) 9 Suppl 4 Suppl 4 (2005), S13-9. issn: 1466-609X. doi: 10.1186/cc3753. url:<http://www.ncbi.nlm.nih.gov/pubmed/16168069%7B%5C%7D5Cn>
- [3] Tang YL, He Y, Shao HW, Mizeva I. Skin temperature oscillation model for assessing vasomotion of microcirculation. Acta Mechanica Sinica. 2015; 31(1): 132-138.
- [4] Martini FH, Nath JL, Bartholomwe EF, Fundamentals of Anatomy and Physiol-

- ogy Ninth Edition, pp. 707-800. isbn-13: 978-0-321-70933-2.
- [5] H. Nilsson. Vasomotion: Mechanisms and Physiological Importance. In: Molecular Interventions 3.2 (2003), pp. 79-89. issn: 1534-0384. doi: 10.1124/mi.3.2.79. url: <http://molinterv.aspetjournals.org/cgi/doi/10.1124/mi.3.2.79>.
- [6] Steven S. Segal. Regulation of blood flow in the microcirculation. In: Microcirculation 12.1 (2005), pp. 33-45. issn: 10739688. doi: 10.1080/10739680590895028.
- [7] Sagaidachnyi et al. Thermography-based blood flow imaging in human skin of the hands and feet: a spectral filtering approach. In: Physiological Measurement 38.2 (2017), pp. 272-288. issn: 0967-3334. doi: 10.1088/1361-6579/aa4eaf. url: <http://www.ncbi.nlm.nih.gov/pubmed/28099162%7B%5C%7D5Cnhttp://-stacks>.
- [8] Mary Jo Geyer et al. Using wavelet analysis to characterize the thermoregulatory mechanisms of sacral skin blood flow. In: Journal of rehabilitation research and development 41.6A (2004), pp. 797-806. issn: 0748-7711. doi: 10.1682/JRRD.2003.10.0159.
- [9] Sagaidachnyi et al. Determination of the amplitude and phase relationships between oscillations in skin temperature and photoplethysmography-measured blood flow in fingertips. In: Physiological measurement 35.2 (2014), pp. 153-66. issn: 1361-6579. doi: 10.1088/0967-3334/35/2/153. url: <http://www.ncbi.nlm.nih.gov/pubmed/24399251>.
- [10] Wei Min Liu et al. Reconstruction of thermographic signals to map perforator vessels in humans. In: Quantitative InfraRed Thermography Journal 9.2 (2012), pp. 123-133. issn: 21167176. doi: 10.1080/17686733.2012.737157.
- [11] J. Grant Mouser et al. A tale of three cuffs: the hemodynamics of blood flow restriction. In: European Journal of Applied Physiology 117.7 (2017), pp. 1493-1499. issn: 14396319. doi: 10.1007/s00421-017-3644-7.
- [12] Anders Eriksen, Dominik Osinski, and Dag Roar Hjelme. Evaluation of thermal imaging system and thermal radiation detector for real-time condition monitoring of high power frequency converters. In: Advances in Manufacturing 2.1 (2014), pp. 88-94. issn: 21953597. doi: 10.1007/s40436-014-0066-1.
- [13] Robert Olbrycht and Boguslaw Wiecek. New approach to thermal drift correction in microbolometer thermal cameras. In: Quantitative InfraRed Thermography Journal 12.2 (2015), pp. 184-195. issn: 21167176. doi: 10.1080/17686733.2015.1055675. url: <http://dx.doi.org/10.1080/17686733.2015.1055675>.
- [14] Wei Min Liu et al. Observing temperature fluctuations in humans using infrared imaging. In: Quant Infrared Thermography Journal 8.1 (2011), pp. 21-36. doi: 10.3166/qirt.8.21-36.
- [15] Akeyede Imam, Usman, Mohammed. and Chiawa, Moses Abanyam. On Consistency and Limitation of paired t-test, Sign and Wilcoxon Sign Rank Test (2014), pp. 01-06. e-issn: 2278-5728, p-issn: 2319-765X. doi: 10.9790/5728-10140106.

VII. APPENDICES

Table 3: Table of blood pressure written into the experimental protocol.

Subject number	1. systolic pressure	2. systolic pressure	3. systolic pressure	Mean pressure	30 % of TOP
1	141 mmHg	138 mmHg	137 mmHg	138.6 mmHg	54.08 mmHg
2	102 mmHg	102 mmHg	102 mmHg	102 mmHg	39.78 mmHg
3	155 mmHg	147 mmHg	146 mmHg	149.3 mmHg	58.24 mmHg
4	138 mmHg	145 mmHg	135 mmHg	139.3 mmHg	54.34 mmHg

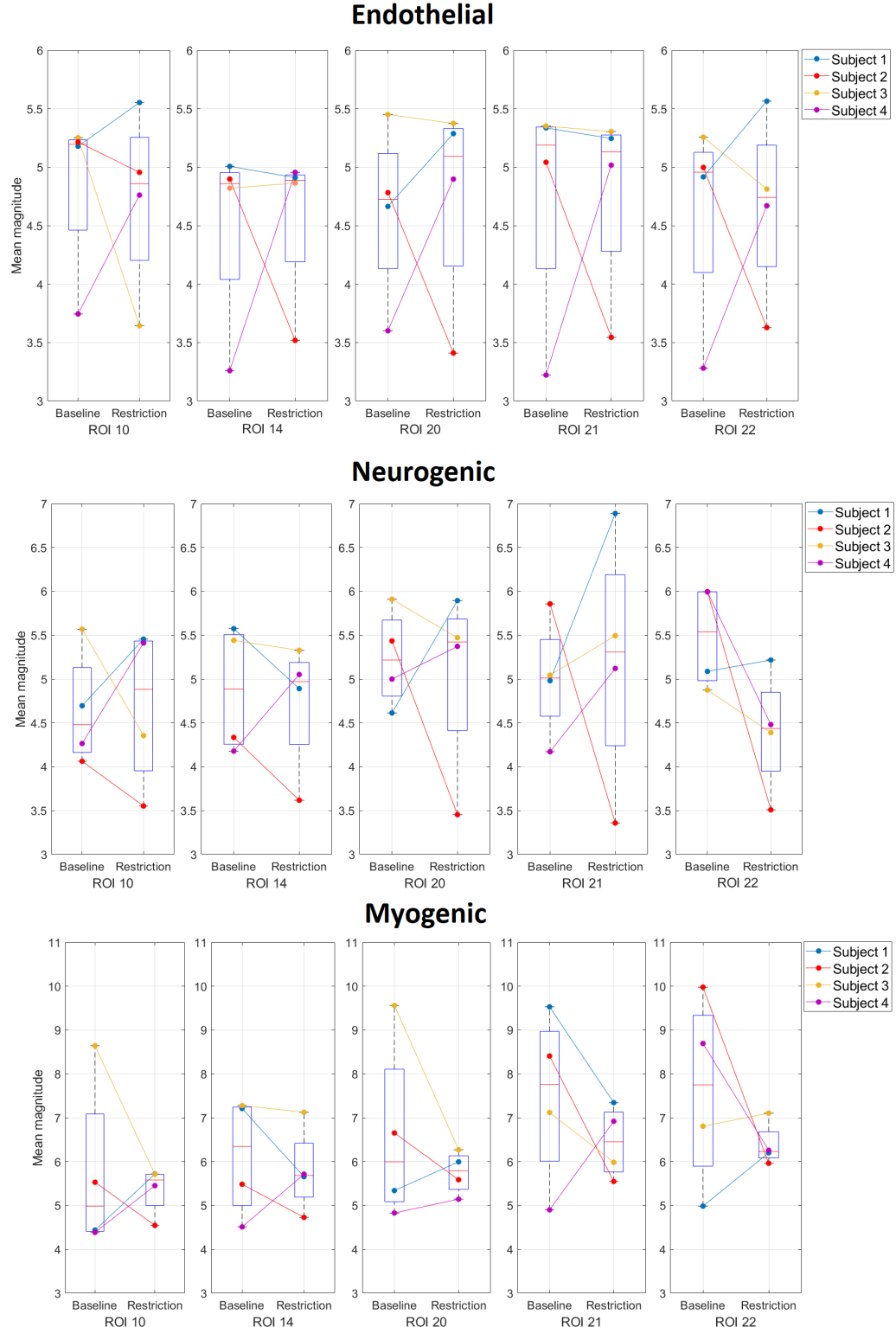


Figure 7: Box plots showing the mean magnitudes for each subject indicated by color within endothelial, neurogenic and myogenic frequency bands for ROI 10, 14, 20, 21 and 22.



AALBORG UNIVERSITET
STUDENTERRAPPORT

Thermal imaging as method to study the effect of induced ischemia on vasomotion

1. Semester project - Fall 2017

Group 7407



1st Semester, Project

School of Medicine and Health

Biomedical Engineering and Informatics

Fredrik Bajers Vej 7A

9220 Aalborg

Title:

Thermal imaging as method to study the effect of induced ischemia on vasomotion

Theme:

Biomedical Signals and Informatics

Project period:

P1, Fall 2017

01/09/2017 - 20/12/2017

Project group:

17gr7407

Participants:

Annabel Bantle

Christian Korfitz Mortensen

Toby Steven Waterstone

Supervisors:

Lasse Riis Østergaard

Carsten Dahl Mørch

Andrei Ciubotariu

Pages: 52

Appendix: 6

Handed in: 20/12/2017

The content of this report is freely available, but publication (with reference) may only be done with agreement with the authors.

Synopsis

Vasomotion is an autoregulatory mechanism that optimizes blood distribution within the microcirculatory system. Thermal imaging is a promising approach to measure this phenomena. Previous studies have detected that vasomotion is quantifiable as temperature micro oscillations in the endothelial (0.005 - 0.02 Hz), neurogenic (0.02 - 0.05 Hz) and myogenic (0.05 - 0.15 Hz) frequency band. Four healthy subjects were recruited to investigate the possibilities of measuring changes in vasomotoric activity caused by partial occlusion of blood supply by using thermal imaging. Measurements were done as a baseline and with 50% restriction of hand's blood supply by brachial cuff. No significant difference between the mean magnitudes of baseline and restriction was found. Results showed thermal imaging might not be sensitive enough to detect changes in vasomotion and limitations in the experimental setup.

Preface

This semester project was conducted by students from Biomedical Engineering and Informatics from Aalborg University in the period of 1st of September until the 20th of December 2017. The theme for the project was "Biomedical Signals and Information". In this project, a study regarding the use of thermal imaging to study the physiological phenomena of vasomotion has been conducted.

The group would like to thank Lasse Riis Østergaard, Carsten Dahl Mørch and Andrei Ciubotariu for supervising this project.

Aalborg University, 20th of December 2017

Contents

Part I Background	1
1 Anatomy and Physiology	2
1.1 Macrocirculatory system	2
1.2 Microcirculatory system	3
2 Hemodynamics	6
2.1 Physiological Base	6
2.2 Physical Base	6
3 Vasomotion in disease	8
3.1 Types of shock	8
3.2 Sepsis and Vasomotion	8
4 Methods of studying vasomotion	10
4.1 Thermal imaging	11
4.2 Laser Doppler flowmetry	12
4.3 Summarizing	12
5 Thermal imaging	13
5.1 Introduction to thermal imaging	13
5.2 Measuring thermal energy	14
Part II Methods	17
6 Experimental setup	18
6.1 Subjects	18
6.2 Test setting	19
6.3 Software setting	20
7 Interpretation of data	21
7.1 Time-frequency analysis	21
Part III Data analysis	24
8 Preparation of data	25
8.1 Dividing recording into frames	25
8.2 Regions of interest	26
8.3 Artifacts in temperature recording	28
8.4 Correction method	28

9 Data processing	33
9.1 Scalogram interpretation	33
9.2 Selection of viable regions	35
9.3 Statistical approach	35
Part IV Results	37
10 Results	38
Part V Appendices	44
A Protocol	45
B Evaluation table	48
C Temperature traces	49

Part I

Background

1 | Anatomy and Physiology

The following chapter will outline the functions of the cardiovascular system and focuses on the microcirculatory part. Furthermore the phenomena of vasomotion will be explained.

1.1 Macrocirculatory system

The main function of the cardiovascular system is the blood supply of the whole body and the transportation of metabolites. The propulsion of this is the heart. It generates the systolic blood pressure through the strength of the left ventricle. The pressure difference between the heart and the periphery emerging from there, ensures the blood flow. The blood flows from regions with high pressure, like the aorta, to regions with low pressure, like the periphery.[1]

The heart supplies the body with blood through the systemic and the pulmonary circuit. The heart regulates the blood allocation with adjustment of stroke volume and heart frequency. The oxygen-rich blood accumulates in the left ventricle, from where the blood is pushed out through the aortic valve into the aorta and spread via the arteries into the whole body. The venous system returns the de-oxygenated blood back to the heart into the right atrium. From there the blood flows into the right ventricle and is pushed out through the pulmonary valve into the lung arteries, where gas exchange of the blood occurs. Subsequent the oxygen-rich blood flows via the pulmonary veins back to the left heart to supply the body.[1]

As mentioned, there are two types of vessels, arteries and veins. The difference between the two types of vessels is that arteries transport the blood away from the heart and veins transport blood to the heart. There are also differences in the structure of arteries and veins. Arteries consist of three different layers, tunica interna, tunica media and tunica externa. The tunica interna consists of vascular endothelium, the tunica media consists of smooth muscle cells and elastic fibres, the tunica externa consists of connective tissue and also elastic fibres. Furthermore, there are two different types of arterial vessels. In arteries of the elastic type prevail the elastic fibres in the tunica media. This allows an abrupt extension of the vessel during the systole and ensuing constriction, due to this the blood is transported. In arteries of the muscular type prevail the muscular fibres in the tunica media. This allows regulation of the lumen by constriction and dilatation, whereby the resistance and the blood flow in the organs is regulated.[1]

Venous vessels are similarly structured like arterial vessels, however they are thinner and have semilunar valves inside, to inhibit back flow inside the vessels. This system is supported by the skeletal muscles which help to hold up blood flow. The arterial and the venous vessel system are connected through the capillary system in the microcirculatory

system.[1]

1.2 Microcirculatory system

The heart and larger arteries and veins are associated with the cardiovascular system, but those are only used for transportation of blood. Instead it is the capillaries that permeate most tissues, which is responsible for the perfusion of tissue. These are the only vessels which permit exchange between the vessel and the surrounding interstitial fluids. Factors that affect tissue perfusion is cardiac output, peripheral resistance and blood pressure. Capillaries form capillary beds. Here they work as a interconnected network of vessels. The arteries decrease in size the further they expand into the peripheral system. The small arteries divide into arterioles which further divide into dozens of capillaries. The capillaries merge into a venule after the blood has been de-oxygenated. A capillary is divided into two segments, first the metarteriole and second the capillary. The blood flow between arterioles and venules can also be a direct connection, made by an arteriovenous anastomosis. This works as a bypass diverting blood flow around the capillary bed. An example of the structure of the capillary bed can be seen on figure 1.1.[1]

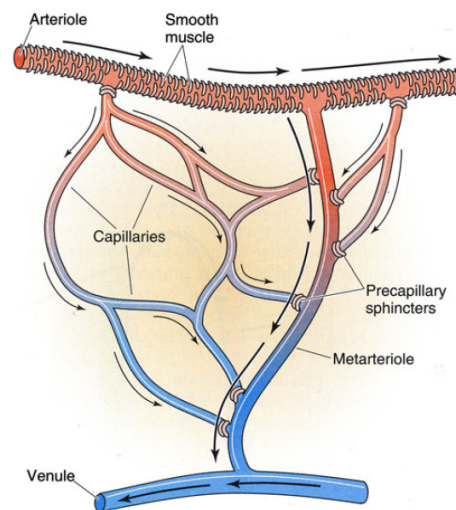


Figure 1.1: The basic structure of a capillary bed, with arteriole over the bed and a venule underneath.[1]

Each capillary entrance is controlled by a precapillary sphincter, which is composed of smooth muscle cells that are able to contract or relax and thereby limit access of blood flow to certain capillaries. This is known as vasomotion. The blood flows relatively slow within the capillaries giving time for the two way exchange of nutrients and wastes.[1]

1.2.1 Vasomotion

The flow within the capillaries varies. This is among other things due to the earlier mentioned precapillary sphincters opening and closing. The opening and closing of sphincters is part of the autoregulation process performed at a local level, to control the blood flow. The vascular system does not contain blood enough for every capillary bed to be filled with blood. Therefore only 25% of the vessel in a capillary bed contains blood, and vessels activity needs to be well coordinated. Thermoregulation and control of nutrition balance are the primary functions of the microcirculatory system. Local changes in concentration of chemicals and interstitial fluids eg. dissolved oxygen concentrations in tissue modulates the vascular smooth muscles activity. Constriction and dilation of the vessel is thereby regulated by this rhythmic activity, also known as vasomotion.[1, 2]

Under normal circumstances cardiac output remains stable and the control of local blood flow happens through local peripheral resistance within local tissues. The regulation of cardiovascular activity is controlled by local homeostatic mechanism. These make sure that demands such as oxygen and nutrients are met and wastes are disposed.[1]

Physiological mechanism controlling vasomotion are not yet fully understood, but vascular smooth muscle activity has been shown to be roughly proportional to the tissue's metabolic demand for oxygen.[2] Studies also suggest that an increase in vasomotion activity enhances oxygen delivery[3]. Furthermore some factors that trigger homeostatic mechanism to alter the vasomotion have been said to have an impact. Factors that trigger dilation is called vasodilators and can be some of the following:[1, 2]

- Decreased O₂ level or increased CO₂ level
- Lactic acid or other acids generated from tissue cells
- NO released from endothelial cells
- Rising concentrations of potassium ions or hydrogen ions in the interstitial fluid
- Chemicals released during local inflammation
- Elevated local temperature

A vasodilation will result in increased oxygen, nutrients, buffers released to recreate homeostasis. Factors that stimulate constriction is called vasoconstrictors and can happen due to following:[1]

- Damaged tissue
- Aggregating platelets

Chapter 1. Anatomy and Physiology

Furthermore mechanisms regulating vasomotion can be divided into three origins. These are endothelial/metabolic, myogenic and neurogenic. Endothelial regulation is based on registered O₂, CO₂, lactate, and H⁺ levels and from this releases nitric oxide as a vasodilator. Myogenic regulation senses strain and stress in vessels, which cause the smooth muscle to depolarize, contracting the vessels. When the ion channels in the smooth muscles close, the blood vessels relaxes leading to vasodilation. Neurogenic signals is said to come from the sympathetic nervous system where these promote vasoconstriction.[4, 5, 6]

2 | Hemodynamics

In this chapter a short introduction to hemodynamics is given to sort out some of the parameters that effect blood flow.

2.1 Physiological Base

The blood pressure is regulated by baroreceptors in the walls of the big arteries in chest and neck area. These receptors register the changes of the elongation of the vessels and transmit this information to medulla oblongata. With the received pressure information initiates the medulla oblongata, if necessary, regulatory measures. The sympathicus is responsible for the short-term regulation. Both, middle-term and long-term regulation, is made by the kidneys. For middle-term regulation messenger substances are released, which entail vasoconstriction. The long-term regulation occurs per pressure diuresis or reabsorption in the kidneys. It is possible to measure different blood pressures at different places in the cardiovascular system, for example the mean arterial pressure (*MAP*). The *MAP* increases in relation to the stroke volume and decreases when blood flows into the peripheral system.[1, 7]

The cardiac output (*CO*) states the blood volume, which is pumped by the heart per time unit (*HR*). The calculation of the *CO* as follows.[1]

$$CO = HR \times \text{strokevolume} \quad (2.1)$$

2.2 Physical Base

To consider the hemodynamics, it is possible to draw similarities by analogy of physical laws. Especially of Ohm's law $R = \frac{U}{I}$ or rather $I = \frac{U}{R}$. A special case of Ohm's law constitutes Hagen-Poiseuille's law in the field of fluid dynamic and rheology. Hagen-Poiseuille's law describes the laminar flow of an homogeneous Newtonian fluid through a rigid pipe depending on characteristics of the fluid and of the pipe.[7, 8]

Blood is an inhomogeneous suspension of liquid and corpuscular components, whose viscosity η depends on more factors than the temperature, and is consequently no Newtonian fluid. Nevertheless it is possible to draw conclusions by analogy of Hagen-Poiseuille's law for the computation of the hemodynamics.[7, 8]

$$\frac{V}{t} = \frac{r^4 \times \pi \times \Delta P}{8 \times \eta \times I} \quad (2.2)$$

Here is the volume flow equivalent to the electrical current *I* and the pressure difference

Chapter 2. Hemodynamics

ΔP to the electric voltage U . Thus, the calculation of the resistance as follows.[7, 8]

$$R = \frac{8 \times I \times \eta}{r^4} \quad (2.3)$$

Thereby volume flow increases 16 times and the resistance decreases 16 times for double radius r .[7, 8]

3 | Vasomotion in disease

This chapter will describe pathologic incidents in the cardiovascular system and organs during shock. Focusing on finding physiological parameters that indicate shock development.

3.1 Types of shock

In general, shock is characterized by hypoxia in tissues due to inadequate blood supply. The hypoxia during a shock leads to the deposition of metabolisms in organs what results in an increased risk of multi organ dysfunction. There are four different types of shocks:[9, 10]

- **Hypovolaemic shock** is caused by a lack of volume. Either as a consequence of blood loss (hemorrhagic shock) or of water, plasma or electrolyte loss.
- **Cardiogenic shock** is caused by cardiac failure, for instance myocarditis, cardiomyopathy in final stage or acute myocardial infarction.
- **Obstructive shock** is caused by obstruction of blood flow, for instance pulmonary embolism, cardiac tamponade or tension pneumothorax
- **Distributive shock** covers, among others, septic shock, anaphylactic shock and neurogenic shock

Main cause for cardiogenic, hypovolaemic and obstructive shock is a decreased cardiac output without adapting the peripheral resistance. This leads to a lack of oxygen supply. Whereas the main cause for a distributive shock lies in a dysfunction of the peripheral areas in terms of reduced systemic vascular resistance as well as varied oxygen extraction.[10]

Shock affects alterations in the microcirculatory system and interferes perfusion[11]. The changes in the circulatory system are in the following section further elaborated with the aid of sepsis.

3.2 Sepsis and Vasomotion

Sepsis is a condition, which develops through systemic inflammatory response syndrome (SIRS) with presence of an infection or bacteria within the body. Sepsis adversely affect heart rate, blood pressure, oxygen extraction and body temperature and leads to multi organ failure in worst cases.[12, 13]

Since sepsis is based on an inflammation, the body activates the inflammatory cascade as an immune response. Some factors released by the inflammatory cascade have influence

Chapter 3. Vasomotion in disease

on vasodilation and triggers a dispersed systemic vasodilation and decrease the responsiveness of the affected vasculature. It is known that sepsis leads to imbalance of the microcirculation, whereby the blood distribution becomes unequal. Areas with a lack of blood supply which already have a need of blood might get less blood, whereas areas with sufficient supply might get more of the available amount of blood. As an adequate oxygen supply requires a sufficient circulation, the condition of the areas with a lack of blood supply deteriorates. If local microcirculation of several organs like kidneys or liver is impaired over time, it leads to failure of these organs.[13, 14]

The vascular endothelium is affected within the incidents of sepsis, because the stressful environments of sepsis activate vascular endothelial cells. Normally it is a protective response, but in sepsis where the disorder remains, this response exaggerates unpredictably. The endothelial probity get lost and causes cell injury and hypoxia. Moreover the tissue underlying the capillaries suffer from the obstructed capillary perfusion and related hypoxia. The scheme in figure 3.1 shows the role of vascular endothelium on the way to organ failure.[14]

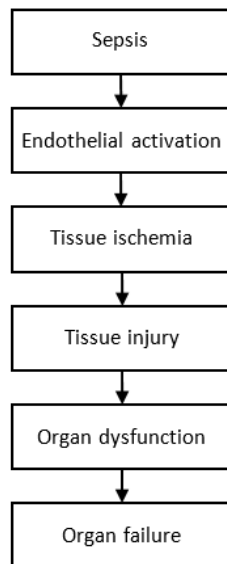


Figure 3.1: Scheme that shows the progression from sepsis to organ failure. Modified from S.Baudouin.[14]

Summarized, sepsis affects the processes within the microcirculation to an extent that the impairment exceed the autoregulation abilities of vasomotion.

4 | Methods of studying vasomotion

In the following chapter an introduction to different techniques of measuring vasomotion will be given. Here methods and applicability for measuring vasomotion will be presented, with main focus directed towards thermal imaging and important parameters in using this technique.

For some time it has been the interest of researchers and health care clinicians to get a better understanding of the mechanisms that control and regulate local blood flow in the microcirculatory system[2, 15, 16, 17]. Visualization of the vessels in skin and the way these behave can be important for assessment of stages of sepsis as mentioned earlier in section 3.1, but also in peripheral vascular disease, the results of skin reconstructive surgery, wound and ulcer management.[13, 17] Spectral components of vasomotion seem to vary when influenced of some diseases. An example could be a decrease in amplitude of endothelial blood flow oscillations is assumed to be a biomarker for endothelial dysfunction. Endothelial dysfunction indicate cardiovascular disorders such as arterial hypertension and cardiac ischemia. An increased amplitude within the neurogenic frequency band is characterized by a decrease of vascular resistance and an increase of blood flow through the arteriovenous shunt.[16]

For measuring regulation in the peripheral blood flow, it is assumed that these oscillating changes are the source of thermal waves propagating from microvessels toward the skin surface. Thermal imaging utilize this concept.[16] Furthermore a correlation between skin temperature in fingertips and blood flow oscillations has been found[15]. When the thermal waves propagate from the vessels towards the skin surface they are prone to some attenuation. This is due to skin properties that function like a low-frequency filter.[18] The magnitude of attenuation is directly proportional to the frequency and the frequency depends on the velocity of the wave propagation[15]. Therefore as illustrated in figure 4.1, a higher frequency leads to a higher attenuation.

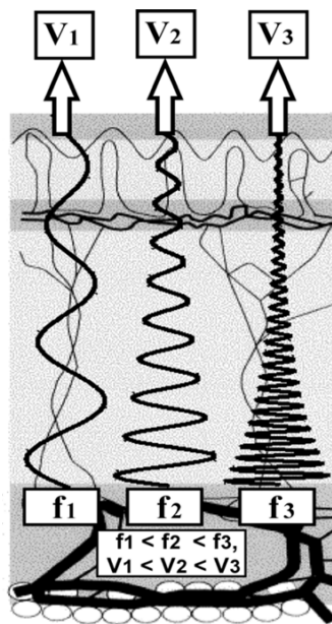


Figure 4.1: Graphical representation of amplitude attenuation through the skin in three signals with different frequency f_1 - f_3 and velocity V_1 - V_3 .[15]

There are multiple different techniques for measuring blood flow in the peripheral circulatory system. For example capillaroscopy, laser Doppler flowmetry (LDF), and thermal imaging. These have been used differently trying to quantify functional aspects of skin vasculature.[17] Laser Doppler flowmetry is one of the most used[2] and thermal imaging being introduced as a new technique of measuring vasoregulation[15].

4.1 Thermal imaging

In studies made by Sagaidachnyi et al. thermal imaging has been used to study vasomotion. In their studies they sought to get better understanding of the relationship between blood flow oscillations and temperature oscillations, and if it was possible to recreate the blood flow oscillations from temperature oscillations. Recordings of blood flow were done by Photoplethysmography and temperature of the skin by thermal imaging. The recordings were made on a small point of the fingertip. Through their work, five frequency bands were identified as vasomotion activity, and are following: endothelial (0.005–0.02 Hz), neurogenic (0.02-0.05 Hz), myogenic (0.05-0.15 Hz), respiratory origin (0.15-0.4 Hz) and cardiac origin (0.4-2.0 Hz).[15, 16] The choice of using thermal imaging to study vasomotion implies certain advantages. Mainly a larger sample area, but also a higher temporal (up to 105 fps) and spatial (2048×1536 pixels) resolution. In addition it is also a non-invasive way of measuring vasomotion.[16]

4.2 Laser Doppler flowmetry

In another study from Geyer et al. vasomotion is investigated through the use of laser Doppler flowmetry as recording technique. In this study, vasoregulation variables are sought quantified. LDF is a non-invasive approach to measuring changes in vasomotion. The technique register changes in the depth of 1 mm, and works like Doppler ultrasound, utilizing the shift in frequency. Though instead of using ultrasonic waves, LDF uses light reflected from red blood cells. This study found the same frequency bands as Sagaidachnyi et al. with minimal difference. Data obtained were analyzed through spectral analysis. Wavelet transform was used instead of the more used Fourier analysis, because wavelet analysis offered better resolution to reveal characteristics in the low frequency area.[2] LDF uses a small sample area and the laser probe allows a sampling area as small as 1 mm³.[19]

4.3 Summarizing

Both Geyer et al. and Sagaidachnyi et al. managed to show spectral components relating to vasomotion. The techniques both used a non-invasive approach. The use of thermal imaging as the method of measuring vasomotion offers interesting opportunities. Larger sampling area would allow interpretation and study of a more global tissue area. Along with the resolution of thermal imaging cameras, this makes thermal imaging the choice of measuring technique to be used in this study.

5 | Thermal imaging

The following chapter will include an introduction to thermal imaging, where general concepts and physical principals will be explained. Furthermore it will be explained how a device measures infrared radiation and converts it into temperature.

5.1 Introduction to thermal imaging

Thermal imaging is a technique that utilizes infrared radiation emitted from nearly any objects. The existence of infrared radiation was first discovered in 1800 by Sir Frederick William Herschel. His experiments lead to the knowledge that there is a light spectrum beyond the visual spectrum humans are able to perceive. Any object above absolute zero emits energy-electromagnetic radiation depending on its temperature.[20, 21]

Infrared radiation is also known as thermal radiation because of the relationship between temperature and infrared radiation. Temperature of the human body permits radiation in the infrared spectrum, but objects of much higher temperature are capable of emitting radiation in the visible and UV spectrum. This has to do with the difference between object and environmental temperature. If the temperature of these are relatively close to each other, the radiation emitted will be within infrared wavelengths. Infrared radiation has a wavelength from 769 nm to 1 mm. Objects emit more radiation in some regions compared to others. Because of this the infrared spectrum is classified in the three regions, near (769 nm - 2.5 μ m), middle (2.5 μ m - 50 μ m) and far infrared (50 μ m - 1 mm). The human body emits most radiation in the far infrared spectrum. Near and middle cameras are mainly used to measure gases.[20]

Thermal imaging is commonly used to calculate surface temperatures. Two important concepts, heat and temperature emerge in the understanding of this. Temperature is a measure for the internal energy within an object and can be defined as the average kinetic energy of the object. Heat is the energy that passes from a warm object to a colder object. Warm objects will decrease in internal energy and cold objects will increase due to the temperature difference and therefore the heat transfer. In the human body, a constant temperature is kept, homeostasis and therefore the temperature will not decrease even though a heat transfer to the surrounding environment occurs. The environmental temperature do have an impact on how large the heat transfer gradient is. If a body is in a cold environment, the emitted heat will be greater than the absorbed. In the same way, if the environment is much warmer than 37°C, a greater absorption than emission will occur and the body will increase in temperature.[20]

5.2 Measuring thermal energy

The theory of the black body is important to understand the absorption and emission of radiation relative to temperature. Because the theory of the black body is used to describe the laws of infrared radiation and its relationship to temperature. The black body is an ideal perfect emitter of infrared radiation because it absorbs all electromagnetic radiation permitted to it. The black body emits the same amount of radiation as it absorbs, the absorption and emission are both equal to one. Spectral emissive power, also denoted E_λ is the energy emitted by a surface in relation to time and range of wavelength. Figure 5.1 shows a graphical illustration of spectral emissive power of the black body for specific wavelengths when the temperature changes.[20]

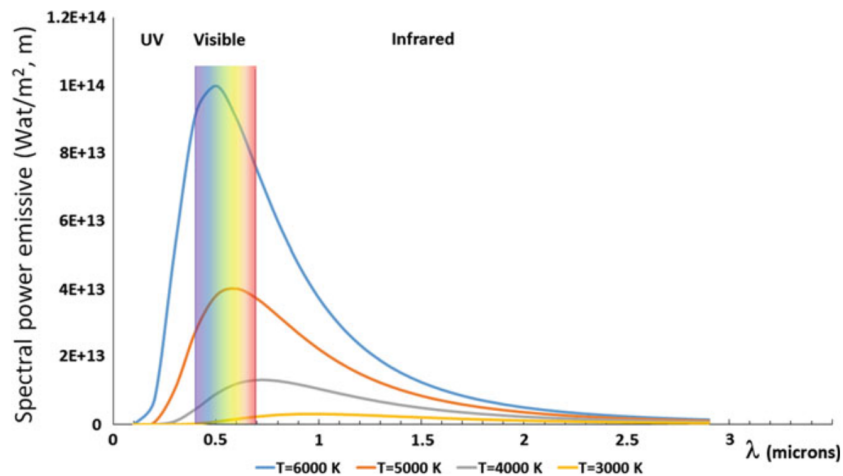


Figure 5.1: Spectral power emissive as a function of wavelength for different temperatures.[20]

The knowledge of this principle helps in the understanding of how infrared radiation behaves, and how temperature affects the wavelength of the signal. The radiation from the human body which has a temperature at 37°C emits the maximum energy of $9.3\mu\text{m}$.[20]

Physical laws including Wien's displacement law and Stefan-Boltzmann's law are important for explaining how the infrared radiation behaves at different temperatures.[20]

Wien's displacement law explains that the wavelength of the peak of the black body radiation curve decreases as the body temperature increases. This law can be used to describe different wavelengths according to the temperature of the black body which emits the radiation. Wien's law has the following equation:[20]

$$\lambda_{max} = \frac{a}{T} \quad (5.1)$$

a has a value of $2.897 \times 10^{-3} \text{ mK}$ and denotes the Wien's displacement constant. T denotes

Chapter 5. Thermal imaging

the absolute temperature in kelvin. λ_{max} denotes the wavelength of emission peak with unit in meters.[20]

Stefan-Boltzmann's law explains that small changes in temperature will lead to big changes in emissive power. This is seen in Stefan-Boltzmann's equation because it states that the total emissive power is proportional to the fourth power of the absolute temperature.[20]

$$E = \varepsilon * \sigma * T^4 \quad (5.2)$$

In Stefan-Boltzmann's equation E denotes the total emissive power with unit W/m^2 . σ denotes the Stefan-Boltzmann's constant, and has a value of $5.67 * 10^{-8} W/m^{-2} K^{-4}$. T is the temperature in kelvin. ε denotes the emissivity and is normally not a part of the Stefan-Boltzmann's law, but part of the modified Stefan-Boltzmann's equation, because it is used for calculation of temperature in most thermal cameras.[20]

Emissivity is different for all materials. Skin has an emissivity between 0.95 and 0.99, why these values typically are used when assessing the temperature of the skin of the human body with thermal imaging. This law is important when considering thermal imaging because the sensitivity when calculating the temperature from the emissive power is considerable.[20]

5.2.1 Thermal cameras

Thermal cameras contain a lens to focus the electromagnetic radiation emitted by an object onto a detector element. A focal plan array (FPA) contains between 384×288 and 1024×768 microbolometers and is often used as detector element in uncooled thermal cameras.[21, 22] The thermal radiation focused by the lens warms up the microbolometers in the FPA. This warming is proportional to the detected radiation. Since microbolometers contain temperature-dependent electric resistance, the voltage of the electrical outcome signal is depending on the detected radiation. The infrared radiation is detected as an analogue signal by the FPA. An AD-converter prepares the signal for the processor module in the thermal camera. The signal is modified into pixels, what gives a digital image as an output, which contains the temperature informations of the observed object. A schematic representation of a thermal detector is illustrated on figure 5.2.[20, 21]

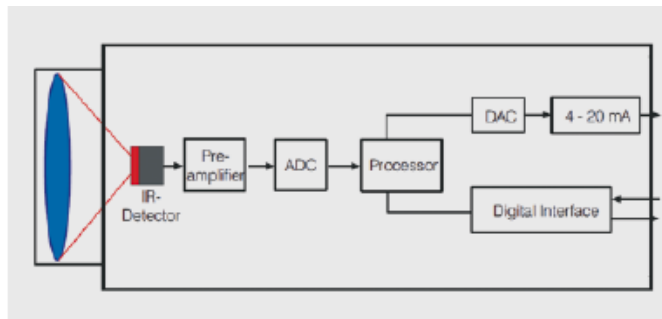


Figure 5.2: Simplified buildup a standard thermal detector.[21]

Part II

Methods

6 | Experimental setup

The following chapter will describe how the experiment is set up, subjects recruited and test and software settings used.

To see if there are changes in the microcirculatory system depending on flow to the observed area, the test was set in two conditions. The first measurement of the hand, was done without intervention, and used as a baseline. The second measurement of the hand was done during a partial occlusion of the blood supply by a brachial cuff. The partial occlusion of the arm leads to ischemia which leads to hypoxia[1]. Aim of the study was to investigate, if there are measurable changes in the micro temperature oscillations of the skin caused by hypoxia in case of shock. Therefore the induced ischemia was used as a way to mimic hypoxia due to shock. The hand was used as observed area. The duration of a measurement was set to 20 min. The lowest frequency of interest is 0.005 Hz with a cycle time of 3 min 20 sec. According to previous studies the recording time was set to 20 min to include six cycles of the lowest frequency.[15] The reason of doing a 50% restriction of blood flow, was due to the intend of creating ischemia without forcing too much discomfort like pain on test subjects, over the 20 min occlusion period. Discomfort test was done prior to the start of the experiment.

By first taking the control measurement under normal conditions, the carry-over effect of occlusion was avoided. It enabled taking both measurements of each subject straight successively, what reduced inaccuracies within the setup of both experiments for each subject. The setting was assembled in the Region Hospital Nordjylland.

6.1 Subjects

Four healthy subjects, three male and one female, with the average age of 30.5 ± 12.5 years were recruited for this experiment. Specific inclusion and exclusion criteria have been formed for this experiment:

Inclusion criteria

- Subjects must be in a normal healthy condition
- Subjects must have at least one hand to perform the experiment on
- The cuff must be able to fit the arm circumference
- The subject must be able to sit still over the 45 min recording period

Exclusion criteria

- Health conditions that set the subject in risk of injury when conducting the experiment.

- Obesity to a greater extend
- Diseases that triggers tremors

6.2 Test setting

The subject was placed in an upholstered chair with adjustable backrest, footrest and armrests, which allowed a good positioning of the measured hand, while the subject remained in a relaxed position. Measurements were carried out on the dominant hand. The hand was stabilized with a vacuum pillow which was covered by a micro fiber tissue to get a better background for the images. Micro fiber has a low heat conduction and therefore prove good contrast[23]. To provide a more comfortable position of the arm during the experiment the armrest of the adjustable chair was padded with some sheets under the vacuum pillow. A comfortable position in the chair was important, because the subject had to sit still and was not allowed to move during the test for at least 45 min. These precautions only counteracted some small movement, and therefore it was important that the subject was focused on sitting still. 37.5 ± 1 cm over the hand the Gobi 640 $17\mu\text{m}$ GigE, sensitivity 0.05° , resolution 480×640 infrared camera (Xenics NV, Belgium) was positioned with a tripod[24]. The setup with camera, chair and computer can be seen on figure 6.1.



Figure 6.1: The test setting at the Region Hospital Nordjylland.

The camera was via an Ethernet cable connected with a laptop, which was used to record the measurements with Xeneth 2.6 software. First cable connections between the camera, the laptop and the power supply were set. Afterwards the camera was turned on and had to warm up for about 15 min[24]. During this the laptop was started and the software for taking the measurements was set in operational readiness.

When the preparation of the test setting was done, the preparation for the subject begun.

At first the blood pressure of the subject was measured on the dominant arm. The blood pressure was measured three times while the subject was sitting relaxed on a chair. Mean systolic blood pressures was calculated. To get the total occlusion pressure (*TOP*) the mean was multiplied by 1.3. To reduce the blood flow in the arm to 50% during the measurement within the second condition, the arm was restricted with 30% of the *TOP*.[25] Then the cuff was affixed at the subjects dominant arm without tightening it, so it was ready for the second part of the experiment. Afterwards the subject took place in the chair and the hand was stabled with the vacuum pillow. The vacuum generator was attached to the pillow for giving the hand more stability. The lens focus has been adjusted so the distance was taken into consideration, to make sure the image was sharp.

When the camera was stable and the filename was modified according to the subject, the first measurement was started for 20 min. During the whole experiment the subject was not allowed to move or speak to minimize movement bias. Directly after the first measurement the cuff on the arm of the subject was tightened with the calculated occlusion value. The pressure of the cuff had to be observed during the whole measurement and if necessary adjusted.

To guide the conductors of the experiment, an experimental protocol was formed and followed during the experiment. The experimental protocol can be seen in chapter A.

6.3 Software setting

To interface the Xenics camera, Xeneth 2.6 software was used. Sampling rate for the thermal imaging camera was set to the lowest possible at 6.25Hz . This should be sufficient according to the Nyquist theory[26], when the frequencies of interest lies within $0.005\text{Hz} - 2\text{Hz}$ as presented in chapter 4. Ambient temperature and room temperature were set to 25° and emissivity to 1.

7 | Interpretation of data

The following chapter will give an introduction to the continuous wavelet transform, and how to interpret the output.

7.1 Time-frequency analysis

Analysis of the collected data from the thermal camera was done in the time-frequency domain. For this a wavelet transformation of the temperature trace was computed in order to look for specific frequency content in the data.

Wavelet transformation is practical when looking for signals of lower frequencies compared to the normal Fourier analysis, because of the bigger resolution in the frequency content. Another drawback of the Fourier transform is the loss of time information, which is preserved with the wavelet transformation.[2]

The CWT is using a variable sized region windowing technique. Long time intervals are used where low frequency information is computed and short time intervals are used where high frequency information is computed. This is represented in figure 7.1.

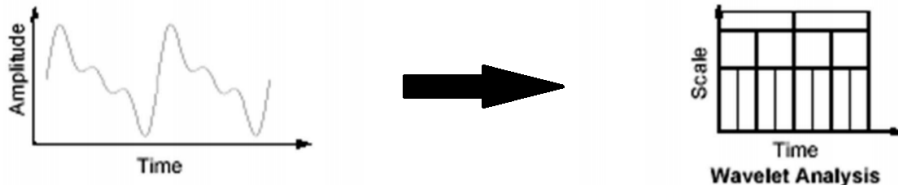


Figure 7.1: Signal in the time domain to frequency domain using the wavelet transformation.
Modified from C.Uvo.[27]

The wavelet transform computes both the scale and time, where the scale being the information of the frequencies and the time being the location. The general form of the CWT is stated in equation 7.1:

$$W(\tau, s) = \int_{-\infty}^{\infty} x(t) \frac{1}{\sqrt{|s|}} \psi * \left(\frac{t - \tau}{s} \right) dt \quad (7.1)$$

Where ψ is the wavelet and $x(\tau)$ is the signal time series.[27, 28] To achieve the CWT, the signal is convoluted with the wavelet to get the wavelet coefficient W for the specific time τ and frequency s . The wavelet coefficient represents the magnitude.

This is done by computing the wavelet of the signal which then is compared to the wavelet for a section at the beginning of the signal. Then the coefficients for the specific frequency and time is calculated for the section of the signal. The wavelet is shifted to the right and repeated until the entire signal is covered. Then the wavelet is scaled and the coefficients is computed for the entire signal again for all frequencies.[27]

Different wavelets can be used to compute the wavelet transformation. In this study the Morlet wavelet is the used wavelet.

The Morlet wavelet is one of the most common wavelets. This wavelet can be seen as analytic, because it has numerical properties and properties of simple conversion from scales to frequencies using equation 7.2.

$$f(s) = \frac{w_\psi}{2\pi s} \quad (7.2)$$

Where w_ψ denotes the central frequency properties of the wavelet.[28]

In MATLAB the cwt(x)-function can be used to compute the CWT by inserting the signal as input. By further defining the sampling frequency in the input, the frequency of the signal content will be displayed. This will give a scalogram as shown in figure 7.2.[29] The frequencies in Hz are shown along the logarithmic y-axis if the sampling frequency is specified, else it will show the normalized frequency in cycles per sample. Along the x-axis is the time vector. The scalogram shows the magnitude of the signal to show how the frequency in the signal is distributed. A scale to see the size of the magnitude is also implied.

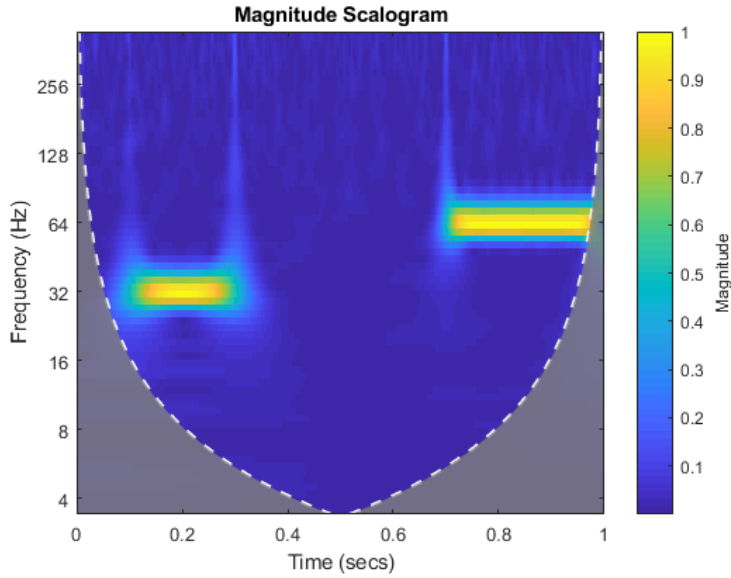


Figure 7.2: An example of a scalogram, showing frequency content at 32 Hz at time approximately 0.2 s and 64 Hz at approximately 0.8 s.[29]

The signal of the wavelet is typically of a finite length, which sets some limitations to the CWT, like the edge effect. The edge effect is an expression of the lack of data, caused by truncation, to calculate specific frequencies because the lower frequencies have bigger windows and thereby require a bigger amount of data to be calculated.[30] The cone of influence (COI) shows the regions of the CWT where edge effects become significant. The gray zone are the areas where the edge effects become significant, which means that there will be some uncertainties to the CWT in this zone.[29]

Part III

Data analysis

8 | Preparation of data

The following chapter will present how the data files from the thermal camera was converted into a temperature traces. Furthermore the chosen regions of interest and applied correction method will be presented.

8.1 Dividing recording into frames

Data acquired from the thermal camera using the Xeneth 2.6 software was saved as an xvi file. These files were read into MATLAB R2017b as an uint16 vector file. Before the frames could be separated from the xvi file, the header in front of the files needed to be excluded. The header contained 307729 data points. With the header removed, the frame separation could be carried out. This was done by first calculating the size of one frame. When knowing that each frame would have the dimensions of 480 x 640 pixels, the size of one frame would correspond to 307200 data points for each frame. It should be considered that each frame also contained a 16 bit header. The number of frames in one recording was calculated by dividing the length of one frame by the entire length of the data file containing all frames, without the file header. The data points for each frame were trimmed for its specific frame header and reshaped from a vector into a matrix and verified by showing the images. An example of a raw image can be seen on figure 8.1. The images contain the pixel intensities of values from 0 to 65535, which is corespondent to the size of the uint16 bit file.



Figure 8.1: Image of one frame from subject 1 after separation.

8.2 Regions of interest

The regions of interest (ROIs) were chosen as pixel locations in the image on specific places of the hand. ROI were selected on behalf of getting a full representation of the hand. Regions in the fingertips and nail folds are areas where it is easy to access the microcirculatory hemodynamics of the human body according to[31].

The raw image on figure 8.1 does not provide very good contrast for identifying ROIs. To easier choose ROIs, the raw image was converted to a gray scale image to improve the contrast in the image, this can be seen in figure 8.2.

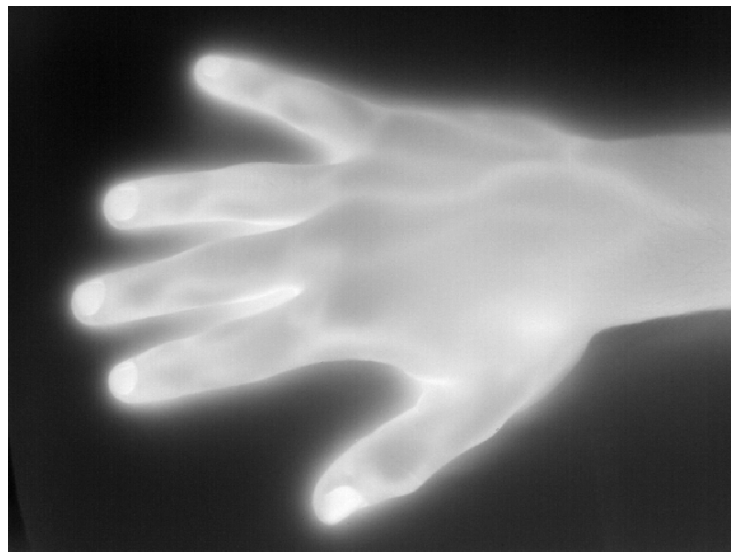


Figure 8.2: High contrast thermal image for subject 1.

With the improved contrast, 28 ROIs from the hand were chosen on the first image of the thermal image series, by finding the coordinates of the pixels in the image. The regions are illustrated on figure 8.3. The localization of the regions is originating from the fingertips and elongating down the hand to the beginning of the wrist. Each region gives a temperature value from one pixel of the image. In the setup of this study one pixel corresponds to an area on the hand with a diameter of about $417\mu\text{m}$. Based on the fact, that the capillaries have an average diameter of $8\mu\text{m}$ [1], it is sufficient to represent each region with just one pixel. Even the area represented by one pixel contains more than one capillary.

Chapter 8. Preparation of data

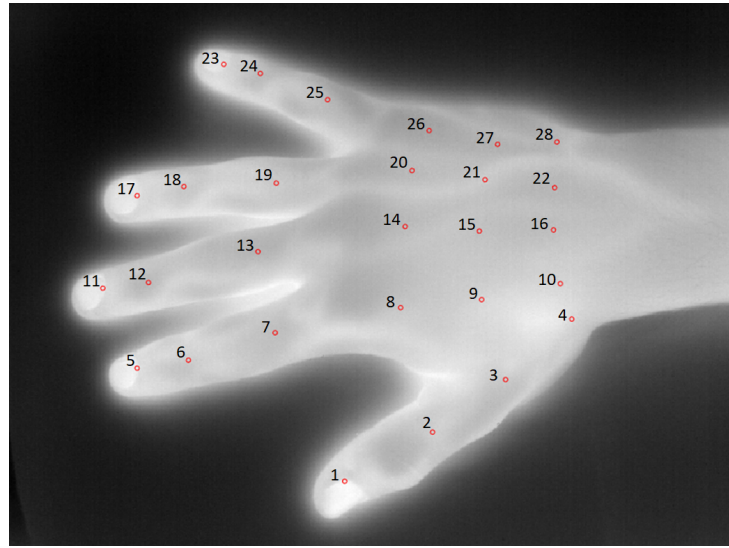


Figure 8.3: First thermal image of subject 1's recording while restriction, with ROI of interest plotted on 28 areas of the hand represented as red circles.

The regions are fixed within the image matrix for the whole image series for each measurement, assuming that the subject was sitting still during the whole data acquisition period. The regions also account for both the baseline and restriction recording for each subject, assuming that the position of the hand was at the same position in both conditions. Iterating over the image series saving ROIs into a cell array with data points for each ROI, a vector for the each of the 28 ROI was made to give the temperature variations over the whole measurement. An example of the temperature for subject 1 is shown on figure 8.4.

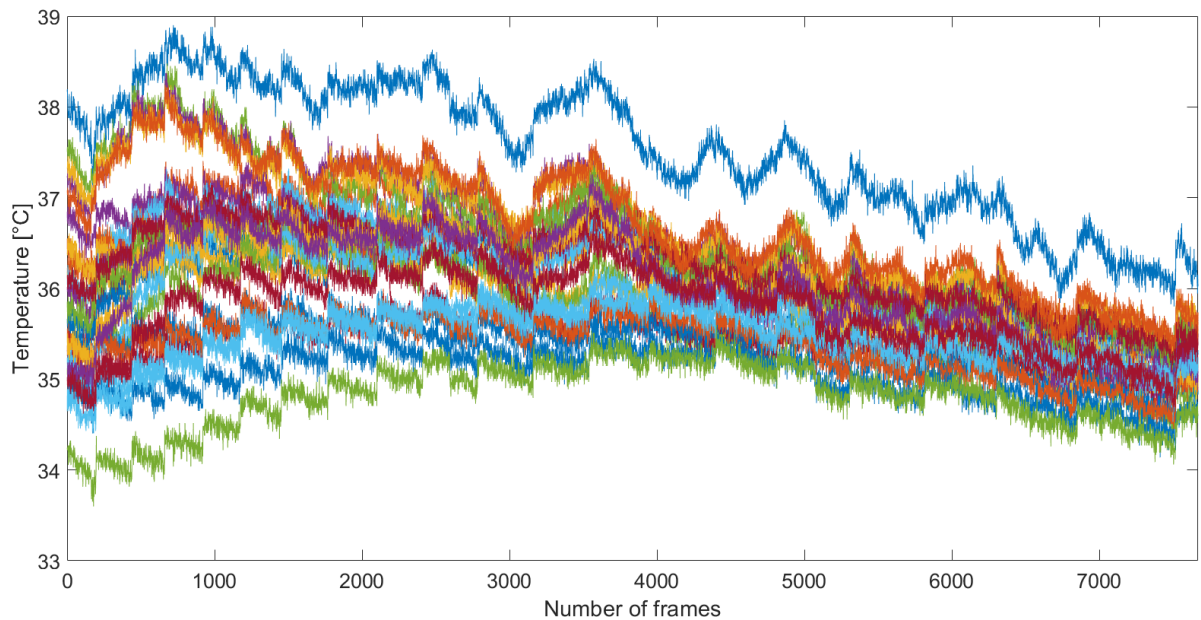


Figure 8.4: Temperature traces for all 28 ROIs during the restriction measurement of subject 1.

8.3 Artifacts in temperature recording

As seen in figure 8.4 the data contain systematic changes which rule out a representation natural temperature variation. Since those changes occur at the same time in different locations of the thermal image, it is assumed that the greater shifts are due to a technical limit. Because of this assumption, it is chosen to further investigate the buildup of thermal cameras and look into other studies to see if they had encountered similar difficulties.

8.3.1 Thermal pixel drift

In a study by Eriksen et al. where thermal imaging was assessed as use for measuring temperature of electrical systems, data recording showed similar behavior. They clearly state that two types of noise is present in their recording. One being white noise from the radiation detector and electronics, and another being a low frequency technical noise. To compensate for these artifacts, a moving average filter was applied.[32] A moving average filter would not be an appropriate correction method, because of the risk of losing the low frequent content of interest.

Thermal cameras are composed of a matrix of microbolometers as mentioned in section 5.2.1. Each microbolometer is also known as a pixel detector for thermal radiation.[22, 33] Unfortunately it shows that these microbolometers are sensitive to noise especially in uncooled cameras, where the internal temperature is not regulated. The noise is formed because each microbolometer has a different response to the same infrared excitation. Furthermore it is assumed by some, that this response is linear[22]. This drift in each microbolometer in the focal plane array is also known as non-uniformity. To achieve radiometric precision the camera has to make a correction for this drift called non-uniformity correction. A common way to recalibrate bolometers is to move a shutter in between the lens and the focal plane array. The shutter has a uniform color which is used to create a new reference for all microbolometers.[22, 33] These auto-adjustments might be what Eriksen et al. saw in their recordings.

Furthermore the drift component is increasing with increasing distance from the center of the thermal image.[22]

8.4 Correction method

With the knowledge of what might be the source of the artifacts seen in the temperature recording, it is chosen to find a way to compensate and correct the recording. Discontinuities occur in each region of interest at the same time and are shown by a high difference in the values between two frames. The amount of the observed discontinuities varies between 0 and 20 in the recordings. Furthermore the appearance of the discontinuities is non-periodic and in each recording at different time points and interval. An example of a trace with discontinuities is seen in figure 8.5.

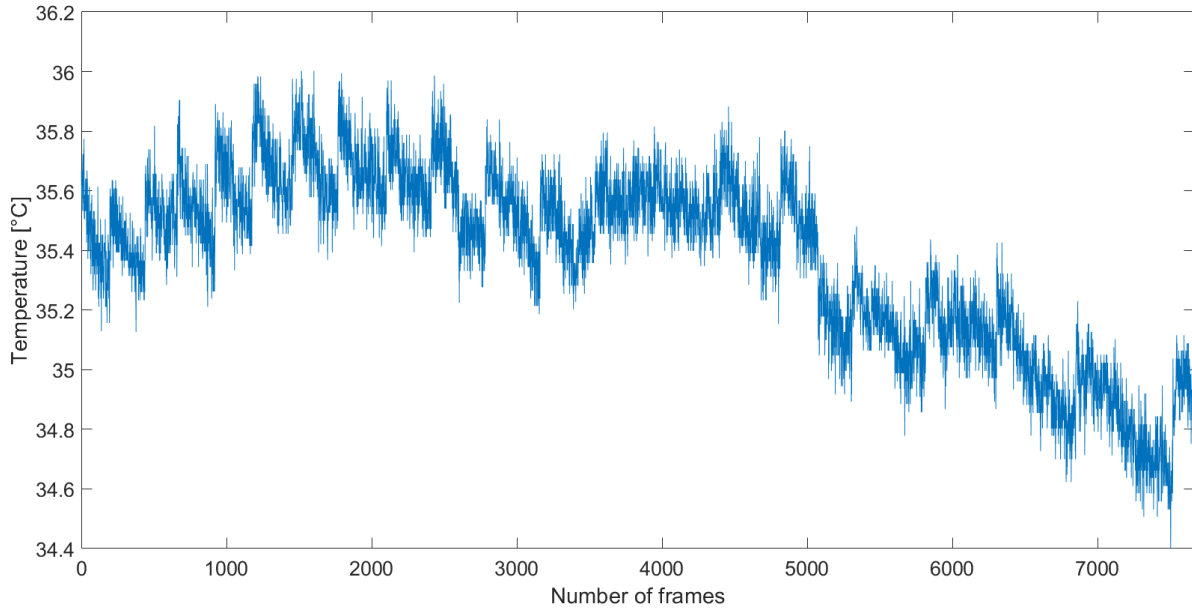


Figure 8.5: Raw trace of region 15 in the restricted recording of subject 1 including 20 discontinuities.

Additionally there is also a drift occurring within each interval between two discontinuities, which hampers the correct data analysis. To reduce the drift component and the discontinuities in the traces, the two following correction methods have been compiled, whereby the second one has been implemented.

8.4.1 Method 1: Regression of first interval

The first implemented method is based on the assumption that the drift is equal in each interval. Therefore a linear regression for the first interval has been made. With the resultant slope m follows the calculation of the drift difference d within the first interval. Due to the assumption, that the drift difference is equal, the slope of the drift of each interval depends on the length of the interval. The slopes have been calculated with equation 8.1.

$$m = \frac{d}{\text{length(interval)}} \quad (8.1)$$

To compensate for the drift, a straight with the inverse slope and starting point in the first data point of the interval has been calculated. The middle points between the raw data and the new calculated straight build the correction of the trace.

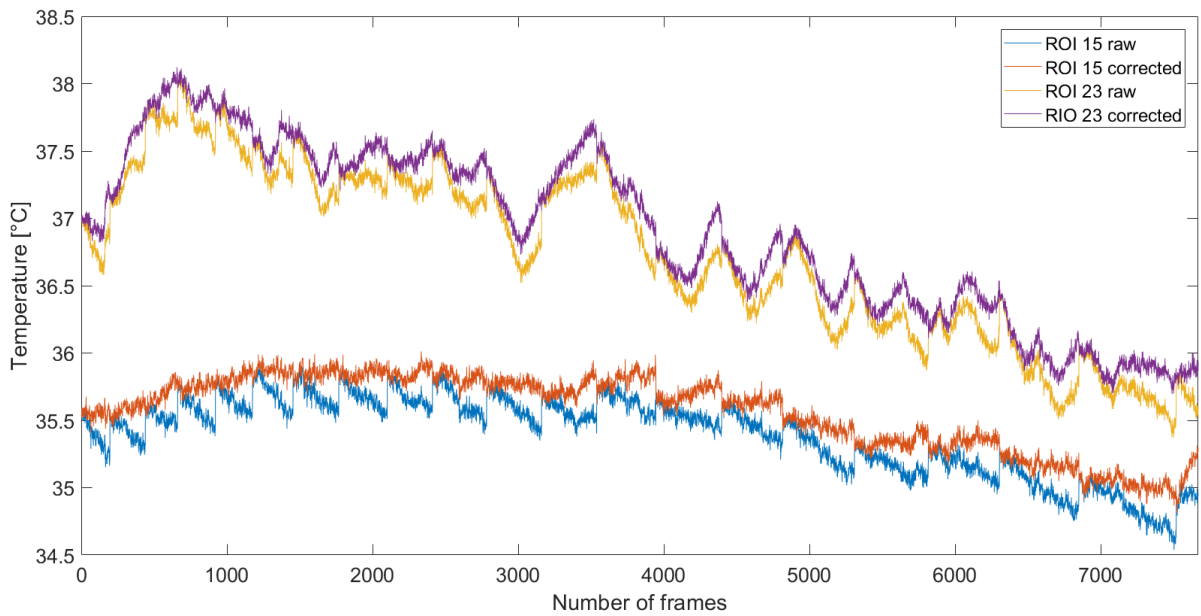


Figure 8.6: Raw trace of ROI 15 in blue and ROI 23 in yellow. Applied correction of ROI 15's data in red and ROI 23's data in purple.

As it can be seen in figure 8.6 this correction only worked partially where several parts showed less drift and lower discontinuities. Through the method worked at some parts it still had a lot of weak points. Primarily because some discontinuities had been strengthened. Due to the effect of the tested correction method, it was chosen to develop another approach.

8.4.2 Method 2: Regression of each interval

The second implemented method is due to the failure of the first method. Out of the recorded data the exact drift is indeterminable. Hence a method which tries to fit the separate intervals together without suppression of the basic shape of the trace has been chosen. Therefore firstly the linear regressions for all intervals and the corresponding residuals are calculated. The idea is to move the end point of a regression line and the start point of the next regression line together. Thus the middle points between end and following start point are calculated. The alignment of the regression lines is changed, so that the start and end points of all the new created orientation straight fit the middle points, except the first and the last orientation straight. Both fit just one middle point. The start of the first orientation straight is the start point of the regression line of the first interval and the end point of the last orientation straight is the end point of the regression line of the last interval.

Chapter 8. Preparation of data

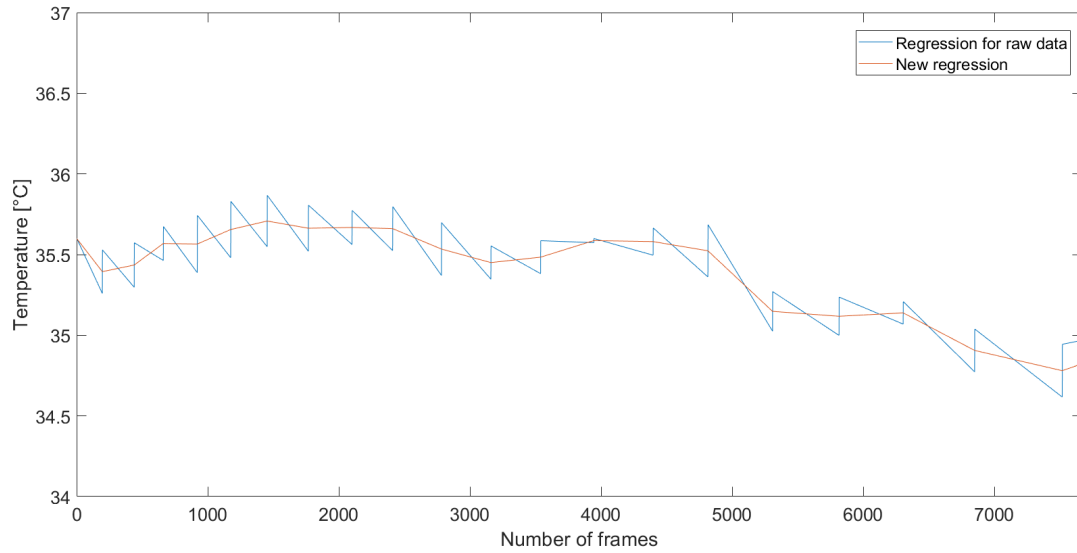


Figure 8.7: Connected regression lines of the raw data of region 15 in the restricted recording of subject 1 in blue. New created orientation line of the same recording in the same region shown in red.

As shown in figure 8.7 the new orientation straight fits the regression lines together without suppressing the shape of the trace. Subsequently the residuals have been added to the new orientation straight, to sustain the ratio between the data points. Figure 8.8 shows the corrected trace wherein the discontinuities, separated intervals, have been connected and the discontinuities have been largely corrected. The corrected and uncorrected temperature traces of all subjects can be seen in appendix C.

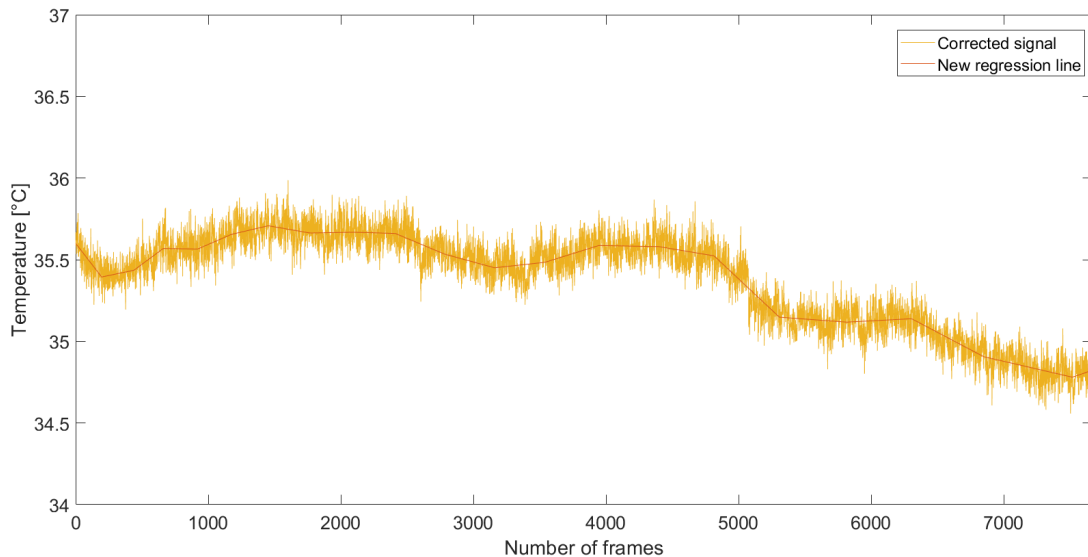


Figure 8.8: Orientation line based on the data of the restricted recording of subject 1 in region 15 shown in red. Corrected trace of the same data in yellow.

However, this method still has weak points. In figures 8.5 - 8.8 ROIs is located in the center of the thermal image. ROI which are located in the outer area of the thermal image show a few discontinuities after the correction, illustrated on figure 8.9. These extended discontinuities are due to the fact that the thermal image is more unstable in the outer areas than in the center, thus the pixel drift is increasing with increasing distance to the center of the thermal image[22]. This means that in the corrected data of ROIs located in the outer areas of the thermal image artifacts still occur.

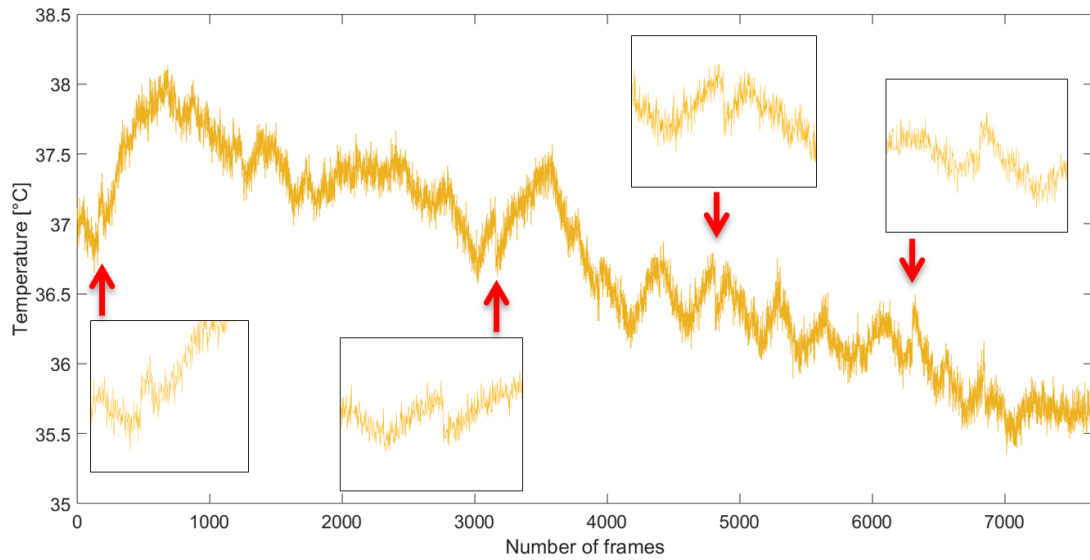


Figure 8.9: Corrected data of the restricted recording of subject 1 in region 23 shown in yellow. Red arrows show the discontinuities in this trace.

9 | Data processing

In the following chapter the outcome of the CWT applied to the corrected temperature trace will be described. A section will present viable ROIs that are chosen for the statistical analysis. Finally it will be explained how the features from the scalograms are extracted and to be tested

9.1 Scalogram interpretation

The data contains the time series of pixel intensities for each of the 28 ROIs for each recording of a subject, which the CWT is computed for after the trace has been corrected. A scalogram showing the time-frequency content of the trace is given as output of the CWT. Frequencies of higher magnitude will show up with brighter colors, which can also be seen on the magnitude colorbar for comparison of the magnitude with related values. The frequency illustrated by the scalograms lies between 2.7370 Hz and 0.0031 Hz. This means, according to the literature, that bands of cardiac, respiratory, endothelial, myogenic and neurogenic is represented in the wavelet frequency span for the time-frequency analysis.[2, 15] An example of a raw uncorrected scalogram is shown figure 9.1 representing the CWT for ROI 8 from subject 3.

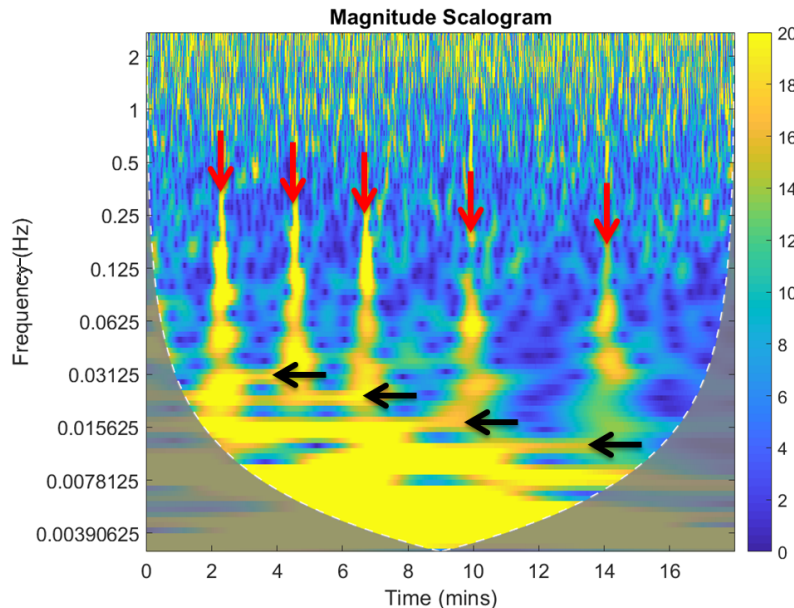


Figure 9.1: Scalogram from the raw trace from ROI 8 in the baseline recording of subject 3. Red arrows mark high spikes. Black arrows mark drifts within the intervals.

Looking at the scalogram from the raw trace in figure 9.1 the discontinuities can easily be seen as bright spikes which represent the discontinuities in the trace. Five discontinuities

that are indicated with the red arrows, are present in the scalogram at time points around 2.5, 4.5, 6.5, 10 and 14 min in the trace. The discontinuities in the same trace shown in the time domain occur at the same time points. It is presumed that the corrected drift also is represented in the scalogram as low frequency content. Hereby different artifact components can be suspected to be included in the trace content.

The artifact components of the raw trace can be sorted into three categories:

- Uniform white noise artifacts
- Drift artifacts within each interval
- Discontinuities

Uniform white noise artifacts is characterized by having the same magnitude in all frequencies. This artifact will therefore not affect the trace of interest, because it will have a flat power spectral density throughout the bandwidth of the frequencies. White noise is independent and evenly distributed[34]. The discontinuities in the trace are induced by the auto-adjustments from the thermal camera described in 8.3. The drift artifacts can be seen as higher magnitudes in the scalogram as lower frequencies than the discontinuities. A frequency band leading up to a spike occur with each discontinuity indicated with black arrows in figure 9.1, indicating that the drift is not uniform between intervals. The artifact components will be disturbing the trace from the micro oscillations to get a representative CWT, because this trace can be hidden by the artifacts. The artifacts are not constant for each recording, why the correction of the trace has been implemented.

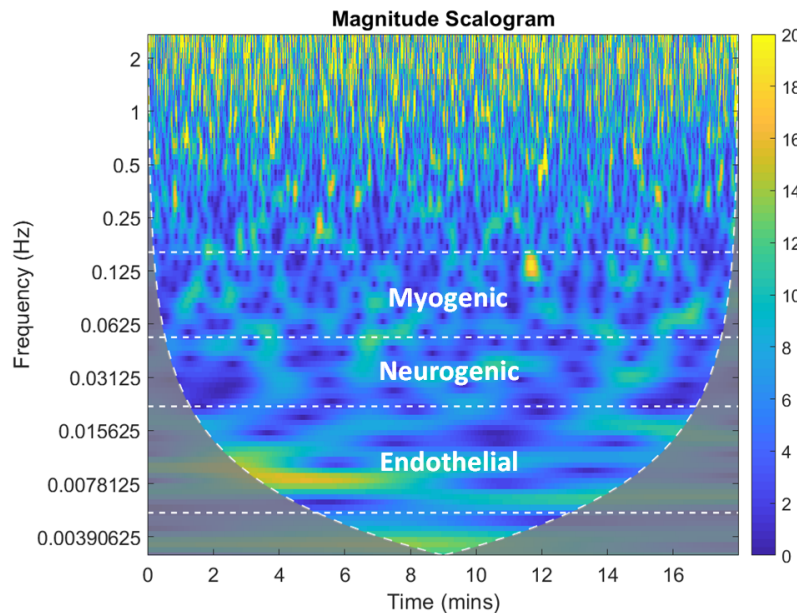


Figure 9.2: Scalogram from the corrected trace of ROI 8 in the baseline recording of subject 3.

After the correction of the trace using method 2, the energy has been reduced in the areas induced from the discontinuities and the drift. The scalogram is left with less energy overall as seen in figure 9.2, which is also showing the range of the endothelial, neurogenic and myogenic frequency bands.

9.2 Selection of viable regions

After application of the correction method, each trace and its scalogram was submitted a manual control. During this control it was noticed that some traces still contained discontinuities which hampers correct data analysis for those traces. A table, which can be seen in appendix B, was used to evaluate each region in each subject within both conditions, concerning the appearance of discontinuities in the trace after applied correction method and usability regarding further data processing.

With the aid of the evaluation table, five ROIs were chosen as valid for further data analysis. The criteria for this selection were, that those ROIs showed good response to the correction method and no discontinuity artifacts were visible shown in the scalogram. An example of this selection is illustrated on figure 9.3. The five selected ROIs are 10, 14, 20, 21 and 22, which are located in the back of the hand and can be seen in figure 8.3.

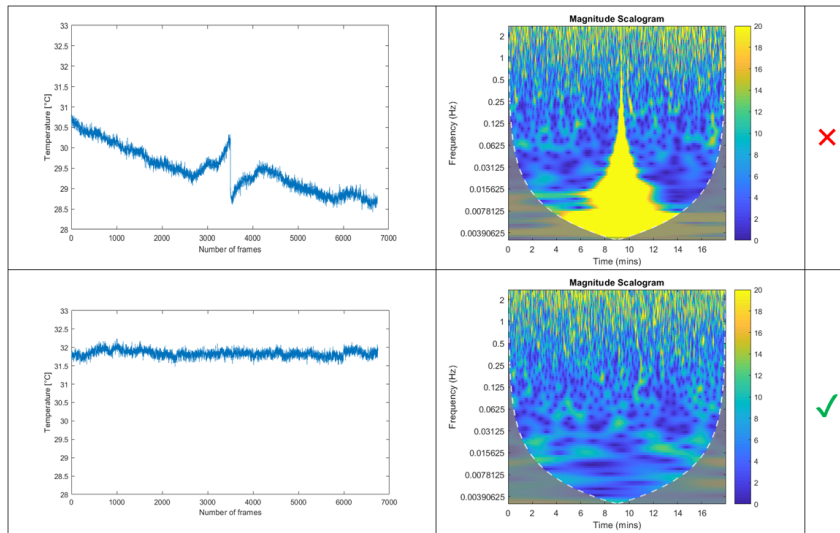


Figure 9.3: Corrected traces from ROI 10 and 23, temperature plot with corresponding scalograms. ROI 23 was excluded and 10 accepted.

9.3 Statistical approach

As the actual distribution of the data is unknown, the statistical approach was based on the assumption that the data is normal distributed due to natural variance within subjects.

It is chosen to test for significant difference between the condition by using a paired t-test on the mean magnitude for a frequency band. Using the mean magnitude as feature for the statistical test build on an approach presented in Liu et al.[35] To prepare the data for the paired t-test, first the average magnitudes for each time period of endothelial, neurogenic and myogenic frequency band were calculated by equation 9.1.

$$W(n_f) = \frac{1}{N} \sum_{n=1}^N W_n(n_f) \quad (9.1)$$

Where N denotes the total number of elements in the frequency band, W is the magnitude of the wavelet, n_f is the respective frame and n is the current element of the magnitude of the frequency band.

Then the mean of the average magnitude over the time period is calculated by equation 9.2.

$$W_{mean} = \frac{1}{N_f} \sum_{n_f=1}^{N_f} W(n_f) \quad (9.2)$$

Where W_{mean} denotes the mean value of the frequency band over the time period and N_f is the total number of frames. This gives a single value for the specific frequency band to use in the statistical test for comparison between the two conditions.

Before a paired t-test was computed, a box plot was shown to get a visual representation of the mean magnitudes within the three frequency bands.

A paired t-test was performed on all five regions. A significance level of 0.05 was used the statistical test.[36]

Part IV

Results

10 | Results

In the following chapter the results from the data analysis will be presented. Box plots and a table will present the mean magnitude values. A paired t-test is used to test the likelihood of finding a significant difference between the two conditions, baseline and restriction.

The box plots can be seen in figure 10.1 throughout figure 10.3. The box plots show points for each mean magnitude for each subject ordered by color, a line is connecting the before and after condition to indicate if there has been an increase or decrease in magnitude.

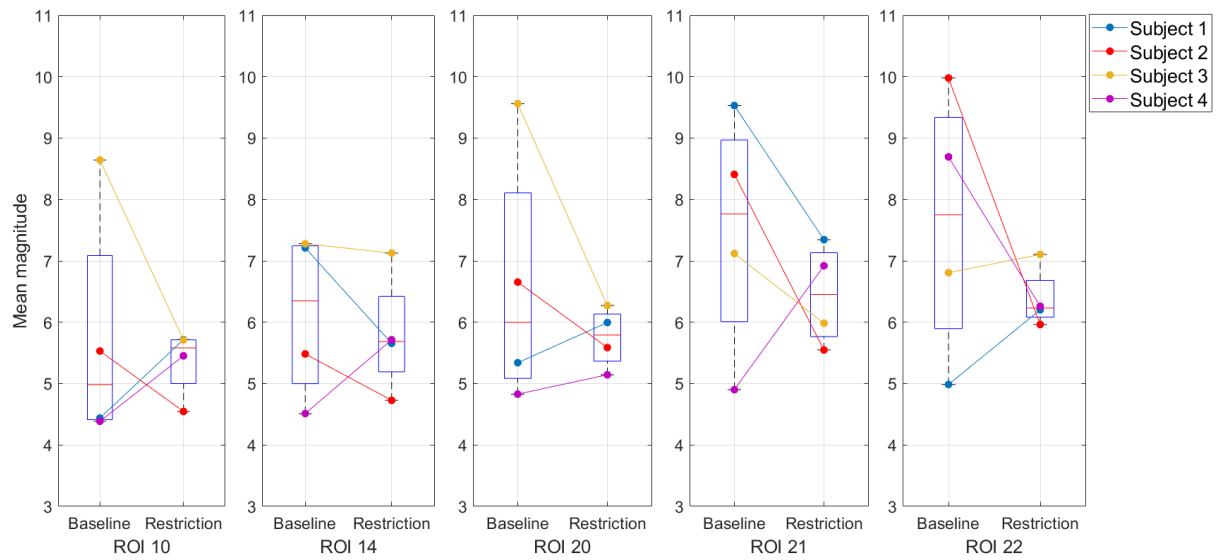


Figure 10.1: Box plot for mean magnitude in the endothelial frequency band, for both conditions in five ROIs.

Chapter 10. Results

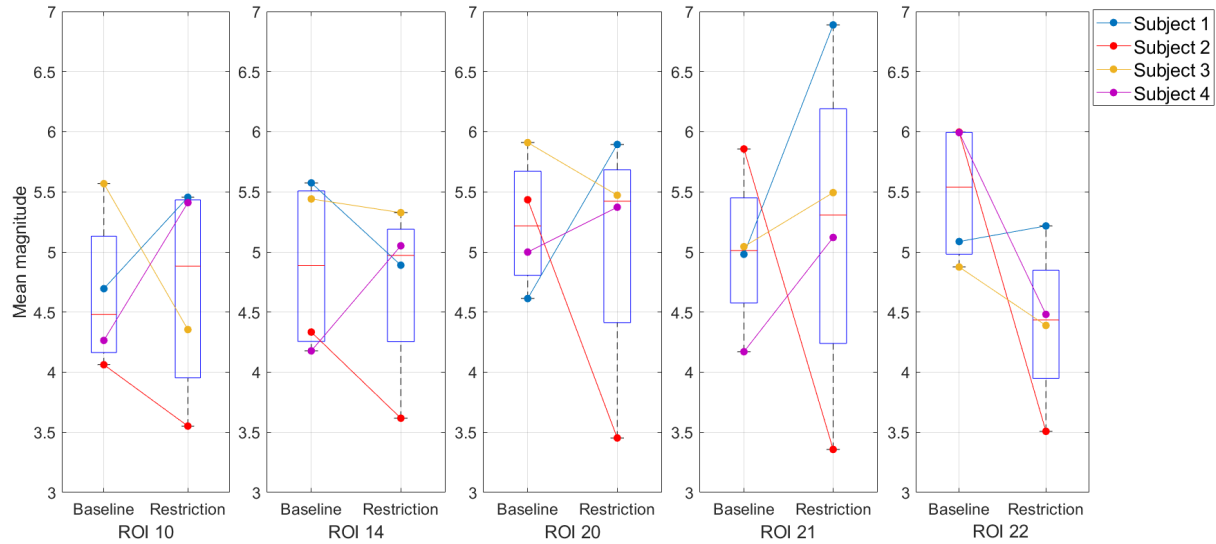


Figure 10.2: Box plot for mean magnitude in the neurogenic frequency band, for both conditions in five ROIs.

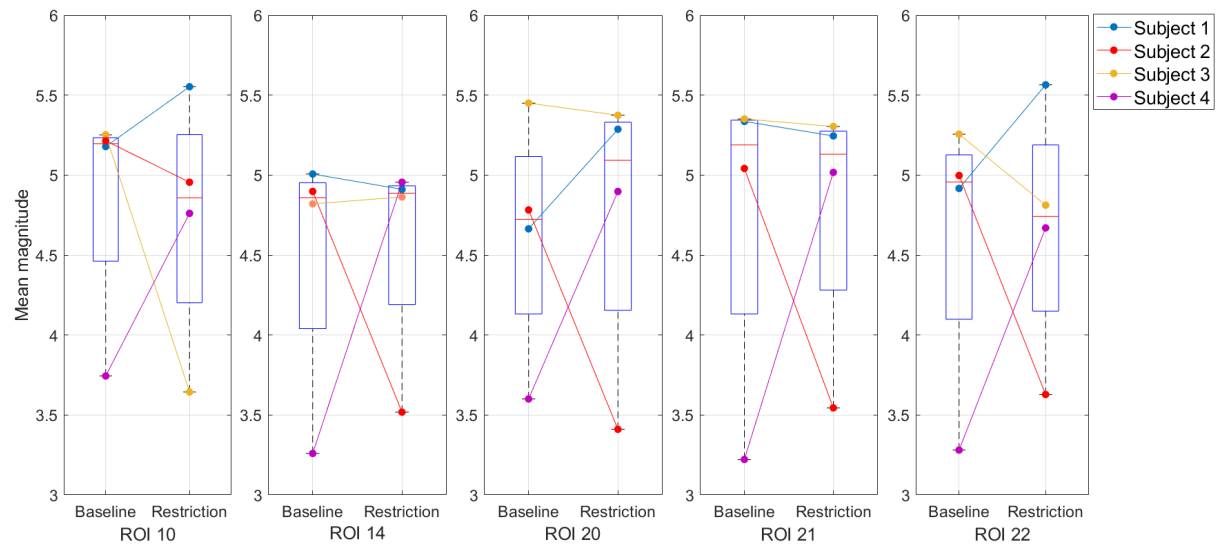


Figure 10.3: Box plot for mean magnitude in the myogenic frequency band, for both conditions in five ROIs.

Table 10.1 illustrates a mean magnitude value for endothelial, neurogenic and myogenic frequency band in the baseline and restricted measurement. The mean magnitude values are representing all subjects and ROIs.

The outcome of the paired t-test is a table showing the p-values, which is shown in table 10.2.

Table 10.1: Table showing the mean magnitudes of each frequency band in both measured conditions.

	mean endo	mean neuro	mean myo
Baseline	6.71±1.90	5.05±0.65	4.66±0.77
Restriction	5.95±0.75	4.82±0.95	4.70±0.72

Table 10.2: Table showing the p-values corresponding to specific ROI in correlation with frequency band.

	p-endo	p-neuro	p-myo
ROI 10	0.71	0.93	0.84
ROI 14	0.62	0.69	0.92
ROI 20	0.41	0.80	0.84
ROI 21	0.40	0.84	0.95
ROI 22	0.38	0.15	0.93

As indicated in table 10.2, all of the tests show a significance level well above 0.05, which means that h_0 is not rejected, whereby there is no significant difference between the two conditions.

Bibliography

- [1] Bartholomew EF Martini FH, Nath JL. *Fundamentals of Anatomy and Physiology Ninth Edition*. Pearson, 2012, p. 1272. ISBN: 13: 978-0-321-70933-2.
- [2] Mary Jo Geyer et al. “Using wavelet analysis to characterize the thermoregulatory mechanisms of sacral skin blood flow.” In: *Journal of rehabilitation research and development* 41.6A (2004), pp. 797–806. ISSN: 0748-7711. DOI: 10.1682/JRRD.2003.10.0159.
- [3] Daniel Goldman and Aleksander S. Popel. “A Computational Study of the Effect of Vasomotion on Oxygen Transport from Capillary Networks”. In: *Journal of Theoretical Biology* 209.2 (2001), pp. 189–199. ISSN: 00225193. DOI: 10.1006/jtbi.2000.2254. URL: <http://linkinghub.elsevier.com/retrieve/pii/S0022519300922549>.
- [4] Steven Segal. “Regulation of Blood Flow in the Microcirculation”. In: *Microcirculation* 12.1 (Feb. 2005), pp. 33–45. ISSN: 1073-9688. DOI: 10.1080/10739680590895028. URL: <http://doi.wiley.com/10.1080/10739680590895028>.
- [5] Can Ince. “The microcirculation is the motor of sepsis.” In: *Critical care (London, England)* 9 Suppl 4. Suppl 4 (2005), S13–9. ISSN: 1466-609X. DOI: 10.1186/cc3753. URL: <http://www.ncbi.nlm.nih.gov/pubmed/16168069%7B%5C%7D5Cnhttp://www.pubmedcentral.nih.gov/articlerender.fcgi?artid=PMC3226164>.
- [6] H. Nilsson. “Vasomotion: Mechanisms and Physiological Importance”. In: *Molecular Interventions* 3.2 (2003), pp. 79–89. ISSN: 1534-0384. DOI: 10.1124/mi.3.2.79. URL: <http://molinterv.aspetjournals.org/cgi/doi/10.1124/mi.3.2.79>.
- [7] Marc Thiriet. *Biology and Mechanics of Blood Flows - Part II: Mechanics and Medical Aspects*. Springer Science, 2008. ISBN: 978-0-387-74848-1. DOI: 10.1007/978-0-387-74849-8.
- [8] Abraham Noordergraaf. *Blood in Motion*. 2011. ISBN: 978-1-4614-0004-2. DOI: 10.1007/978-1-4614-0005-9.
- [9] Marie Dam Lauridsen et al. “Positive predictive value of International Classification of Diseases, 10th revision, diagnosis codes for cardiogenic, hypovolemic, and septic shock in the Danish National Patient Registry”. In: *BMC Med Res Methodol* 15 (215). URL: <https://www.ncbi.nlm.nih.gov/pmc/articles/PMC4373092/>.
- [10] Daniel Vincent, Jean-Louis; De Baker. “Circulatory Shock”. In: *N Engl J Med* 369.Critical Care Medicine (2013), pp. 1726–1734. URL: <http://www.nejm.org/doi/full/10.1056/NEJMra1208943>.
- [11] Ronald V. Maier. “Approach to the Patient with Shock”. In: *Harrison’s Principles of medicine* 18 (2012). URL: <http://accessmedicine.mhmedical.com/content.aspx?bookid=331%7B%5C%7Dsectionid=40727056>.
- [12] Robert H. Shmerling Ryszard M. Pluta. “Sepsis”. In: 308.20 (2010), p. 7424.

- [13] Saowanee Kanta, Boonyang Plangklang, and Wanchai Subsingha. "World ' s largest Science , Technology & Medicine Open Access book publisher c". In: *Energy Procedia* 56.C (2014), pp. 604–609. ISSN: 9789533070865. DOI: 10.5772/711.
- [14] Simon V. Baudouin. *Sepsis: Introduction and Epidemiology*. 2008, pp. 1–2. ISBN: 9781846289385. DOI: 10.1007/978-1-84628-939-2_1.
- [15] Sagaidachnyi et al. "Determination of the amplitude and phase relationships between oscillations in skin temperature and photoplethysmography-measured blood flow in fingertips." In: *Physiological measurement* 35.2 (2014), pp. 153–66. ISSN: 1361-6579. DOI: 10.1088/0967-3334/35/2/153. URL: <http://www.ncbi.nlm.nih.gov/pubmed/24399251>.
- [16] Sagaidachnyi et al. "Thermography-based blood flow imaging in human skin of the hands and feet: a spectral filtering approach". In: *Physiological Measurement* 38.2 (2017), pp. 272–288. ISSN: 0967-3334. DOI: 10.1088/1361-6579/aa4eaf. URL: <http://www.ncbi.nlm.nih.gov/pubmed/28099162%7B%5C%7D5Cnhttp://stacks.iop.org/0967-3334/38/j=2/a=272?key=crossref.169506a8780bc72b4d9d219e09a28a32>.
- [17] Wei Min Liu et al. "Reconstruction of thermographic signals to map perforator vessels in humans". In: *Quantitative InfraRed Thermography Journal* 9.2 (2012), pp. 123–133. ISSN: 21167176. DOI: 10.1080/17686733.2012.737157.
- [18] Sergey Podtaev, Matvey Morozov, and Peter Frick. "Wavelet-based correlations of skin temperature and blood flow oscillations". In: *Cardiovascular Engineering* 8.3 (2008), pp. 185–189. ISSN: 15678822. DOI: 10.1007/s10558-008-9055-y.
- [19] Matthew R Brothers et al. "Methodological assessment of skin and limb blood flows in the human forearm during thermal and baroreceptor provocation". In: *J Appl Physiol* 109 (2010), pp. 895–900. ISSN: 8750-7587. DOI: 10.1152/japplphysiol.00319.2010.â€ťSkin.
- [20] Jose Ignacio et al. *Application of Infrared Thermography in Sports Science*. 2017, pp. 49–79. ISBN: 978-3-319-47409-0. DOI: 10.1007/978-3-319-47410-6. URL: <http://link.springer.com/10.1007/978-3-319-47410-6>.
- [21] Optris. "Basic principles of non-contact temperature measurement". In: (2009), pp. 1–7. URL: www.optris.com/applications?file=tl%7B%5C%7Dfiles/pdf/.../IR-Basics.pdf.
- [22] Robert Olbrycht and Boguslaw Wiecek. "New approach to thermal drift correction in microbolometer thermal cameras". In: *Quantitative InfraRed Thermography Journal* 12.2 (2015), pp. 184–195. ISSN: 21167176. DOI: 10.1080/17686733.2015.1055675. URL: <http://dx.doi.org/10.1080/17686733.2015.1055675>.
- [23] L. Schacher, D.C. Adolphe, and J.-Y. Drean. "Comparison between thermal insulation and thermal properties of classical and microfibres polyester fabrics". In: *International Journal of Clothing Science and Technology* 12.2 (2000), pp. 84–95. URL: <https://doi.org/10.1108/09556220010371711>.
- [24] Xenics nv. *User Manual Gobi-640-17µm GigE/CL/CXP Camera and Gobi-384-25µm GigE/CL Camera*. 2012, p. 29.

Bibliography

- [25] J. Grant Mouser et al. “A tale of three cuffs: the hemodynamics of blood flow restriction”. In: *European Journal of Applied Physiology* 117.7 (2017), pp. 1493–1499. ISSN: 14396319. DOI: 10.1007/s00421-017-3644-7.
- [26] Martin H. Weik. *Nyquist sampling rate*. 2000. DOI: 10.1007/1-4020-0613-6_12653. URL: https://link.springer.com/referenceworkentry/10.1007/1-4020-0613-6%7B%5C_%7D12653.
- [27] Cintia Bertacchi Uvo. “Fourier and Wavelets Transforms”. In: (1995), pp. 1–19.
- [28] Luís Aguiar-Conraria and Maria Joana Soares. “The Continuous Wavelet Transform: A Primer”. In: *NIPE-Universidade do Minho* (2011), pp. 1–43. URL: http://www.economics-ejournal.org/economics/journalarticles/2011-16/references/@@export%7B%5C%7D5Cnhttp://www.eeg.uminho.pt/economia/nipe%7B%5C%7D0A*.
- [29] MathWorks. *Continuous 1-D wavelet transform*. 2017. URL: https://se.mathworks.com/help/wavelet/ref/cwt.html?searchHighlight=cwt%7B%5C&%7Ds%7B%5C_%7Dtid=doc%7B%5C_%7Dsrchtitle (visited on 01/01/2017).
- [30] Françoise Coppens Jean-Luc Mari, F. Glangeaud. *signal processing for geologists and geophysicists*. illustrere. Editions Technip, 1999, p. 458. ISBN: 2710807521, 9782710807520.
- [31] M. L. Iabichella, E. Melillo, and G. Mosti. “A Review of Microvascular Measurements in Wound Healing”. In: *The International Journal of Lower Extremity Wounds* 5.3 (2006), pp. 181–199. ISSN: 1534-7346. DOI: 10.1177/1534734606292492. URL: <http://journals.sagepub.com/doi/10.1177/1534734606292492>.
- [32] Anders Eriksen, Dominik Osinski, and Dag Roar Hjelme. “Evaluation of thermal imaging system and thermal radiation detector for real-time condition monitoring of high power frequency converters”. In: *Advances in Manufacturing* 2.1 (2014), pp. 88–94. ISSN: 21953597. DOI: 10.1007/s40436-014-0066-1.
- [33] Alejandro Wolf, Jorge E. Pezoa, and Miguel Figueroa. “Modeling and compensating temperature-dependent non-uniformity noise in IR microbolometer cameras”. In: *Sensors (Switzerland)* 16.7 (2016), pp. 1–13. ISSN: 14248220. DOI: 10.3390/s16071121.
- [34] T. Hida and Si Si. “Lectures on White Noise Functionals”. In: (2014), pp. 13–62.
- [35] Liu Wei-Min et al. “Observing temperature fluctuations in humans using infrared imaging”. In: 27.3 (2015), pp. 320–331. ISSN: 09652140. DOI: 10.1002/nbm.3066. Non-invasive. arXiv: NIHMS150003.
- [36] Jerrold H. Zar. *Biostatistical Analysis*. Internatio. Pearson, 2014, p. 751. ISBN: 1-292-02404-6.

Part V

Appendices

A | Protocol

Experimental Protocol

Experiment

Study of temperature oscillations in the peripheral circulation with infrared thermography

Formalities

Date:	17.10.2017 and 18.10.2017
Place:	Regionshospital Nordjylland in Hjørring
Conducted by:	Toby Waterstone, Christian Mortensen, Annabel Bantle, Andrei Ciubotariu

Background

Aim:	The aim of the experiment is to measure vasomotion in the hand in two conditions
Type of study:	Quantitative research
Subjects:	<p>Number of subjects: 4</p> <p>Inclusion criteria:</p> <ul style="list-style-type: none">• Subjects should have at least one hand to perform the measure on• The cuff should be able to fit the arm circumference• The subject should be able to sit still for a greater extend of time• Health conditions that sets the subject in risk of injury when conducting the experiment like high blood pressure.• Age under 18 years old• Age over 60 years old• Obesity to a greater extend• Diseases that triggers tremors <p>Exclusion criteria:</p>

Experimental Protocol

Test Requirements

Materials:	Xenics Gobi 640 17μm GigE Infrared camera with power cord, Tripod, Cuff, Chair, Computer with recording software and power cord, Vacuum pillow, Vacuum pump, Stopwatch, Ethernet cable, Computer.
Setup:	
Preparation:	<ol style="list-style-type: none"> 1. The camera has to warm up for 15 min. 2. During this laptop, software and all cable connections should be set in operational readiness.
Procedure:	<ol style="list-style-type: none"> 1. Systolic pressure is measured and mean is calculated 2. Pressure to be used in cuff is calculated 3. The cuff is affixed at the subjects dominant arm without tighten it. 4. The subject can take place in the chair. 5. The hand is put on the vacuum pillow. 6. The vacuum pump is attached to the pillow. 7. The camera needs to be positioned 37.5 cm over the hand with the focus adjusted. 8. If the camera is stable, the first measurement can be started for exact 20 min. 9. Save file as subject_number of subject. 10. Tighten the cuff on the arm of the subject with XXX, without moving the subjects hand. 11. The second measurement can be started for exact 20 min. 12. Maintain same pressure for 20 min. 13. Save file as subject_number of subject_cuff

Appendix A. Protocol

Table A.1: Table of blood pressure written into the experimental protocol.

Subject number	1. systolic pressure	2. systolic pressure	3. systolic pressure	Mean pressure	30 % of TOP
1	141 mmHg	138 mmHg	137 mmHg	138.6 mmHg	54.08 mmHg
2	102 mmHg	102 mmHg	102 mmHg	102 mmHg	39.78 mmHg
3	155 mmHg	147 mmHg	146 mmHg	149.3 mmHg	58.24 mmHg
4	138 mmHg	145 mmHg	135 mmHg	139.3 mmHg	54.34 mmHg

B | Evaluation table

ROI	S1_U	S1_C	S2_U	S2_C	S3_U	S3_C	S4_U	S4_C
1	✗	✗	✓	✗	✗	✓	●	✗
2	✓	✓	✓	✓	✗	✓	✓	✓
3	✓	✓	✓	✓	✗	✓	✓	✓
4	✓	✓	✓	✓	✗	●	✓	✓
5	✗	✗	✓	✗	✗	✓	✓	✗
6	●	●	✓	✓	✗	✓	✓	✗
7	✓	✓	✓	✓	✗	✓	✓	✓
8	✓	✓	✓	✓	✓	✓	●	✓
9	✓	✓	✓	✓	●	✓	✓	✓
10	✓	✓	✓	✓	✓	✓	✓	✓
11	✗	✗	✓	✗	✗	✓	✓	✗
12	✓	✓	✓	✓	✗	✓	✓	●
13	✓	✓	✓	✓	✗	✓	✓	✓
14	✓	✓	✓	✓	✓	✓	✓	✓
15	✓	✓	✓	✓	✗	●	✓	✓
16	✓	✓	✓	✓	✗	●	✓	✓
17	●	✗	✓	✗	✗	✓	✓	✗
18	✓	✓	✓	✗	✗	✓	✓	●
19	✓	✓	✓	✓	✗	✓	✓	✓
20	✓	✓	✓	✓	✓	✓	✓	✓
21	✓	✓	✓	✓	✓	✓	✓	✓
22	✓	✓	✓	✓	✓	✓	✓	✓
23	●	✗	✓	✗	✗	✓	✓	✗
24	●	●	✓	✗	✗	✓	✓	✗
25	●	✓	✓	✓	✗	✓	✓	✓
26	✓	✓	✓	✓	●	✓	●	✓
27	✓	✓	✓	✓	✗	✓	●	✓
28	✓	✓	✓	✓	✗	✓	✓	✓

Legend

✓	ROI in this recording useful
●	ROI in this recording maybe useful
✗	ROI in this recording not useful
■	ROI used for data analysis
■	ROI is improper for data analysis
■	ROI cannot be used for data analysis

Appendix C. Temperature traces

C | Temperature traces

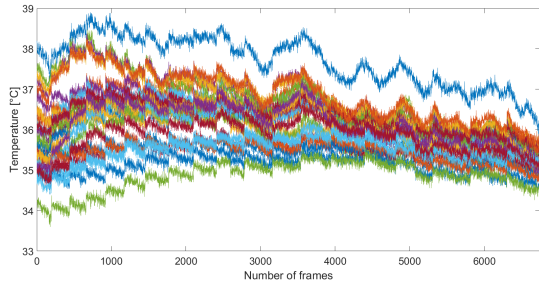


Figure C.1: Subject 1 baseline, uncorrected recording.

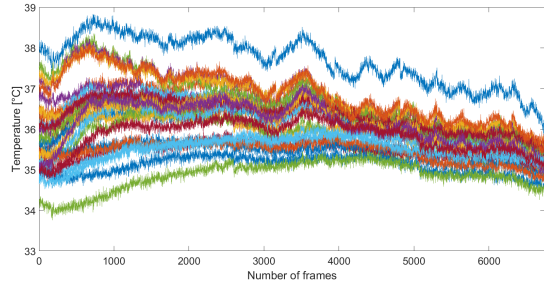


Figure C.2: Subject 1 baseline, corrected recording.

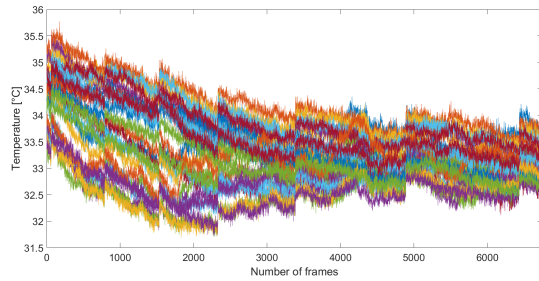


Figure C.3: Subject 1 restricted bloodflow, uncorrected recording

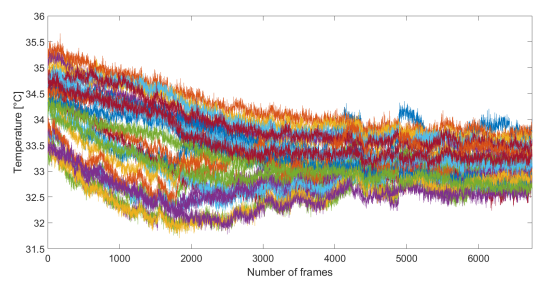


Figure C.4: Subject 1 restricted bloodflow, corrected recording.

Appendix C. Temperature traces

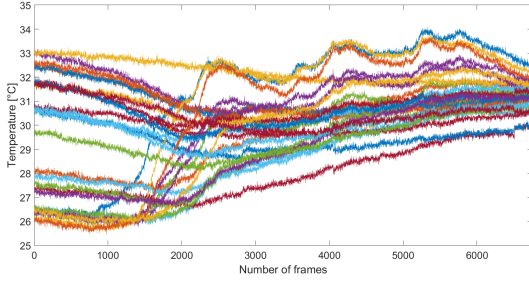


Figure C.5: Subject 2 baseline, raw recording.

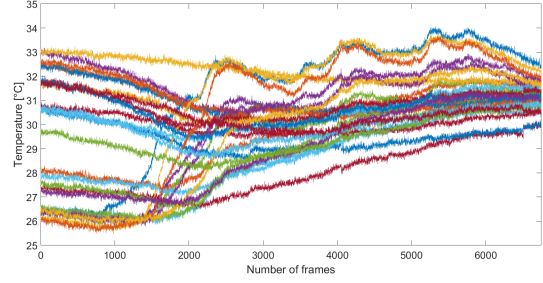


Figure C.6: Subject 2 baseline, no discontinuities in the raw recording.

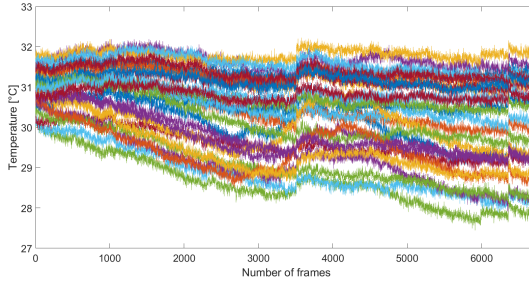


Figure C.7: Subject 2 restricted bloodflow, uncorrected recording.

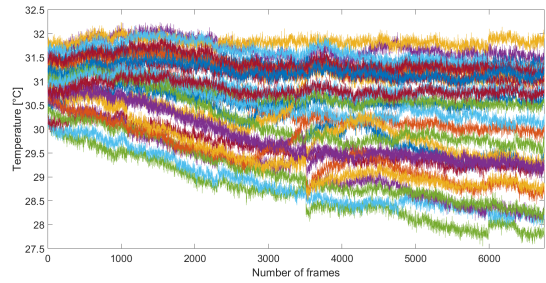


Figure C.8: Subject 1 restricted bloodflow, corrected recording.

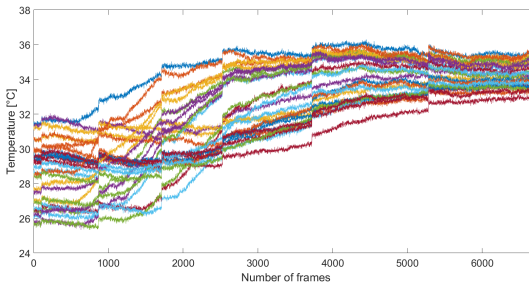


Figure C.9: Subject 3 baseline, uncorrected recording.

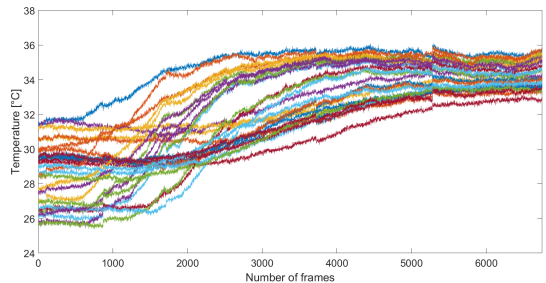


Figure C.10: Subject 3 baseline, corrected recording.

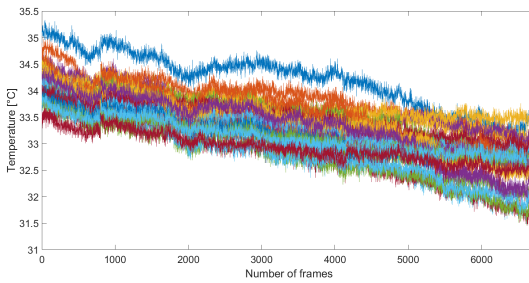


Figure C.11: Subject 3 restricted bloodflow, uncorrected recording.

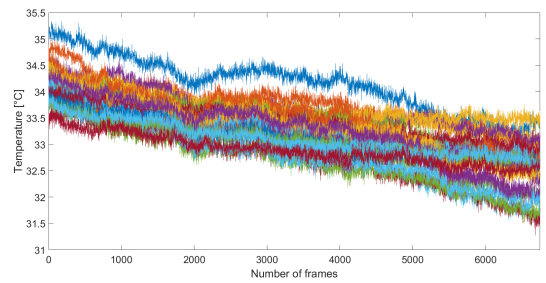


Figure C.12: Subject 3 restricted bloodflow, corrected recording.

Appendix C. Temperature traces

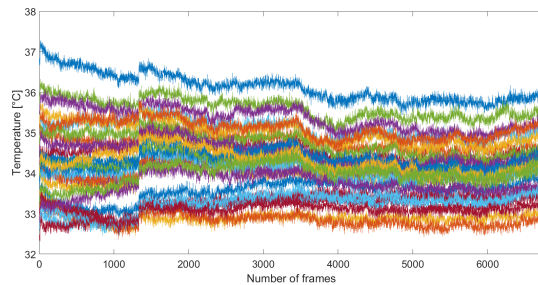


Figure C.13: Subject 4 baseline, uncorrected recording

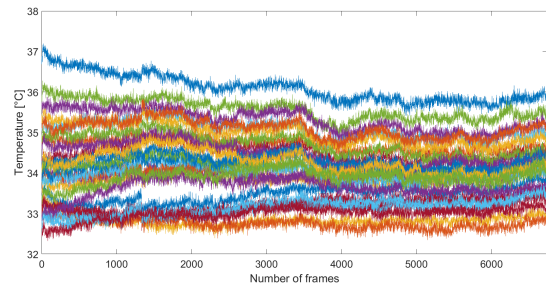


Figure C.14: Subject 4 baseline, corrected recording.

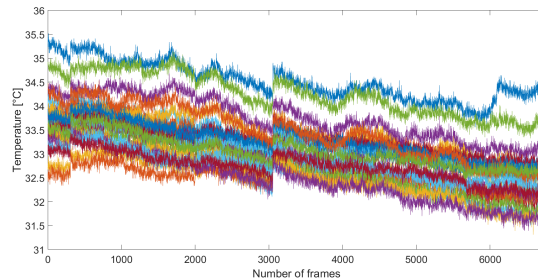


Figure C.15: Subject 4 restricted bloodflow, uncorrected recording

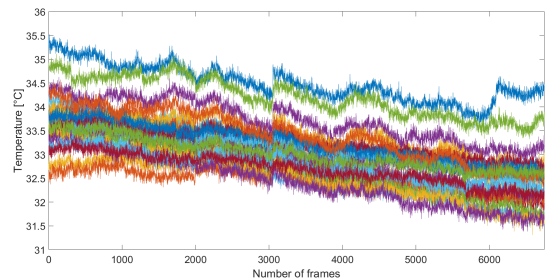


Figure C.16: Subject 4 restricted bloodflow, corrected recording.